

Accumulation of Peptidoglycan O-Acetylation Leads to Altered Cell Wall Biochemistry and Negatively Impacts Pathogenesis Factors of *Campylobacter jejuni*^{*[5]}

Received for publication, July 8, 2016 Published, JBC Papers in Press, July 29, 2016, DOI 10.1074/jbc.M116.746404

Reuben Ha^{†1}, Emilisa Frirdich[‡], David Sychantha[§], Jacob Biboy[¶], Michael E. Taveirne^{||2}, Jeremiah G. Johnson^{||3}, Victor J. DiRita^{||4}, Waldemar Vollmer[¶], Anthony J. Clarke[§], and Erin C. Gaynor^{†5}

From the [†]Department of Microbiology and Immunology, University of British Columbia, Vancouver, British Columbia V6T 1Z3, Canada, the [§]Department of Molecular and Cellular Biology, University of Guelph, Guelph, Ontario N1G 2W1, Canada, the [¶]Centre for Bacterial Cell Biology, Institute for Cell and Molecular Biosciences, Newcastle University, Newcastle upon Tyne NE2 4AX, United Kingdom, and the ^{||}Department of Microbiology and Immunology, University of Michigan Medical School, Ann Arbor, Michigan 48109

Campylobacter jejuni is a leading cause of bacterial gastroenteritis in the developed world. Despite its prevalence, its mechanisms of pathogenesis are poorly understood. Peptidoglycan (PG) is important for helical shape, colonization, and host-pathogen interactions in *C. jejuni*. Therefore, changes in PG greatly impact the physiology of this organism. O-acetylation of peptidoglycan (OAP) is a bacterial phenomenon proposed to be important for proper cell growth, characterized by acetylation of the C6 hydroxyl group of *N*-acetylmuramic acid in the PG glycan backbone. The OAP gene cluster consists of a PG O-acetyltransferase A (*patA*) for translocation of acetate into the periplasm, a PG O-acetyltransferase B (*patB*) for O-acetylation, and an O-acetylpeptidoglycan esterase (*ape1*) for de-O-acetylation. In this study, reduced OAP in $\Delta patA$ and $\Delta patB$ had minimal impact on *C. jejuni* growth and fitness under the conditions tested. However, accumulation of OAP in $\Delta ape1$ resulted in marked differences in PG biochemistry, including O-acetylation, anhydromuropeptide levels, and changes not expected to result directly from Ape1 activity. This suggests that OAP may be a form of substrate level regulation in PG biosyn-

thesis. Ape1 acetyltransferase activity was confirmed *in vitro* using *p*-nitrophenyl acetate and O-acetylated PG as substrates. In addition, $\Delta ape1$ exhibited defects in pathogenesis-associated phenotypes, including cell shape, motility, biofilm formation, cell surface hydrophobicity, and sodium deoxycholate sensitivity. $\Delta ape1$ was also impaired for chick colonization and adhesion, invasion, intracellular survival, and induction of IL-8 production in INT407 cells *in vitro*. The importance of Ape1 in *C. jejuni* biology makes it a good candidate as an antimicrobial target.

Campylobacter jejuni is a leading bacterial cause of food-borne gastroenteritis in the developed world and the most common infectious antecedent to the autoimmune acute polyneuropathy Guillain-Barré syndrome (1, 2). As a commensal of the avian gut, it is a prevalent contaminant of uncooked poultry (3). Because of its high incidence rate, the costs of *C. jejuni* infection are a significant socioeconomic burden, making it both a health care concern and an economic issue (4). In addition, *C. jejuni* has been exhibiting alarming increases in resistance to ciprofloxacin and erythromycin, the most commonly used antibiotics for treatment of *C. jejuni* infection (5). Despite its prevalence, relatively little is known about *C. jejuni* pathogenesis in humans. Traditional virulence factors present in other gastrointestinal pathogens are either absent (*i.e.* dedicated type III secretion systems) or limited (*C. jejuni* possesses some stress-response elements such as the stringent response modulator SpoT, but it lacks several hallmark stress-response elements like RpoS and RpoE), or their role in pathogenicity is debated (*i.e.* the cytolethal distending toxin and a putative type IV secretion system on the pVIR plasmid) (6–11). However, factors considered to be fundamental aspects of bacterial physiology such as metabolism, stress response, and cell shape are hypothesized to play important roles in *C. jejuni* pathogenesis (12, 13).

The peptidoglycan (PG)⁶ sacculus is a heteropolymer of the bacterial cell wall composed of alternating β -1–4 *N*-acetylglu-

^{*} This work was supported in part by Canadian Institutes of Health Research Grants MOP-68981 (to E. C. G.) and TGC-114045 (to A. J. C.), Wellcome Trust Grant 101824/Z/13/Z (to W. V.), and National Institutes of Health NIAID Grant AI069383 (to V. J. D.). The authors declare that they have no conflicts of interest with the contents of this article. The content is solely the responsibility of the authors and does not necessarily represent the official views of the National Institutes of Health.

[✂] Author's Choice—Final version free via Creative Commons CC-BY license.

^[5] This article contains supplemental text S1 and S2 and Tables S1 and S2.

¹ Supported by a Natural Sciences and Engineering Research Council Canada Graduate Scholarship.

² Supported in part with federal funds from the United States Department of Agriculture NIFA Grant 2012-67012-19704 and National Center for Advancing Translational Sciences Grant UL1TR000433. Present address: Dept. of Biological Sciences, North Carolina State University, Raleigh, NC 27695.

³ Supported by National Institutes of Health Molecular Mechanisms of Microbial Pathogenesis Training Program Grant T32 AI007528 and United States Department of Agriculture, National Institute for Food and Agriculture, Grants 2010-65201-20594 and 2013-67012-21136. Present address: Dept. of Microbiology and Molecular Genetics, Michigan State University, East Lansing, MI 48824.

⁴ Present address: Dept. of Microbiology and Molecular Genetics, Michigan State University, East Lansing, MI 48824.

⁵ To whom correspondence should be addressed: Dept. of Microbiology and Immunology, University of British Columbia, Vancouver, British Columbia V6T 1Z3, Canada. Tel.: 604-822-2710; Fax: 604-822-6041; E-mail: egaynor@mail.ubc.ca.

⁶ The abbreviations used are: PG, peptidoglycan; OAP, O-acetylation of peptidoglycan; MurNAc, *N*-acetylmuramic acid; LT, lytic transglycosylase; anHMP, anhydromuropeptide; pNPAC, *p*-nitrophenyl acetate; DICM, differential interference contrast microscopy; PCA, principal component analysis; MEM, minimum essential medium; DOC, deoxycholate; Gm, gentamicin; KS, Kolmogorov-Smirnov; MH, Mueller-Hinton; Cm, chloramphenicol; Km, kanamycin.

cosamine (GlcNAc) and *N*-acetylmuramic acid (MurNAc) residues cross-linked to adjacent strands by peptides bound to the MurNAc residue. It is responsible for providing structural strength to the cell, enabling it to resist changes in osmotic pressure, and for maintenance of cell shape (14–16). The corkscrew motility of *C. jejuni* generated by its helical shape and polar flagella is thought to be important in enhancing its ability to move through viscous media, such as the mucous layer of the gastrointestinal tract (14, 17). Deletion of PG hydrolase enzymes Pgp1 and Pgp2 in *C. jejuni* has led to a change in morphology from helical to straight with accompanying defects in traits associated with pathogenesis, including motility in soft agar, biofilm formation, and chick colonization. PG isolated from Δ *pgp1* and Δ *pgp2* also exhibited altered stimulation of host cell NOD receptors, and Δ *pgp1* elicits an enhanced proinflammatory IL-8 response from INT407 epithelial cells upon infection (18, 19). Changes in PG biosynthesis and composition as well as the release of PG products have long been known to affect physiological and pathogenic properties of many bacterial species (20), including *Listeria monocytogenes* (21, 22), *Helicobacter pylori* (23), and *Streptococcus pneumoniae* (24). Current research continues to support this concept (15). Some recent studies have shown that changes in morphology and PG structure in *Mycobacterium tuberculosis* affect its physiology and virulence in mice (25); changes in morphology in *Proteus mirabilis* affect its swarming motility (26); and changes in morphology in *Helicobacter pylori* alter its motility and colonization potential (27, 28).

Understanding PG biosynthetic mechanisms in *C. jejuni* may prove advantageous to the development of new antimicrobials. It has been suggested that O-acetylation of peptidoglycan (OAP) machinery may be an attractive target (29–33). OAP occurs in both Gram-positive and Gram-negative bacteria and is characterized by the addition of an acetyl group to the C6 hydroxyl group of MurNAc in the PG glycan backbone (Fig. 1A). This modification confers resistance to lysozyme (34, 35), which cleaves β -1,4-glycosidic bonds between MurNAc and GlcNAc (36). Despite the intrinsic resistance to lysozyme provided by the outer membrane of Gram-negative bacteria, lysozyme resistance was shown to be important in *H. pylori* using mutants defective in OAP addition and similar glycan modifications (37). These strains showed increased susceptibility to physiologically relevant concentrations of lysozyme in the presence of the host lactoferrin, which has membrane permeabilization properties (38, 39). O-Acetylated gonococcal PG is implicated in the development of arthritic symptoms and is hypothesized to be attributable to increased PG hydrolase resistance leading to large fragments of circulating PG (40). In addition, OAP is believed to be involved in the regulation of PG turnover by inhibiting endogenous lytic transglycosylase (LT) activity. LTs require an unmodified MurNAc C6 hydroxyl moiety to cleave β -1,4-glycosidic bonds between MurNAc and GlcNAc, generating anhydromuropeptides (anhMPs). LTs are therefore important for generating insertion sites for newly synthesized muropeptides during cell growth and division (41).

The OAP gene cluster was initially identified in *Neisseria gonorrhoeae* and was found to be responsible for OAP in many Gram-negative pathogens (42). It consists of a putative trans-

membrane protein, PG O-acetyltransferase A (PatA) predicted to be involved in the translocation of acetyl moieties from a cytoplasmic source into the periplasm, a periplasmic transferase, PG O-acetyltransferase B responsible for O-acetylation of MurNAc, and a periplasmic O-acetylpeptidoglycan esterase (Ape1) for MurNAc de-O-acetylation (Fig. 1A and B) (42–44). Since their discovery, PatB and Ape1 from *N. gonorrhoeae* and *Neisseria meningitidis* have been well characterized biochemically, including descriptions of the catalytic residues, mechanism of enzyme activity, and substrate specificity (30, 32, 43, 45). The availability of a recently solved crystal structure for *N. meningitidis* Ape1, recently identified Ape1 inhibitors, and studies showing reduced septicemia in mice infected with *N. meningitidis* *ape1* mutants lend support for the application of Ape1 as an antimicrobial target (31, 33, 46).

C. jejuni encodes previously unstudied homologs of the OAP genes *patA*, *patB*, and *ape1*. In this work, the roles of these genes in PG O-acetylation and overall PG biosynthesis, as well as biological and pathogenic attributes were assessed via construction of strains deleted for each or all of these genes followed by biochemical and phenotypic analyses. Each mutant exhibited changes in PG O-acetylation consistent with predicted gene product functions. The accumulation of O-acetylated PG was found to be detrimental to *C. jejuni* fitness, whereas diminished O-acetylation had little to no effect. Δ *ape1* exhibited defects in PG muropeptide composition, cell morphology, pathogenic attributes, and host-pathogen interactions, whereas Δ *patA*, Δ *patB*, and Δ *oap* mutants exhibited no or, in rare cases, only minimal defects for these phenotypes.

Results

C. jejuni OAP Genes Were Identified by BLAST and Mutant and Complemented Strains Were Generated—The OAP gene cluster was identified in *C. jejuni* 81-176 wild type by BLAST analysis using the *N. gonorrhoeae* OAP gene sequences. The loci identified were *cjj81176_0640*, *cjj81176_0639*, and *cjj81176_0638* for *patA*, *patB*, and *ape1*, respectively (Fig. 1B). Amino acid sequence identity and sequence similarity for these genes were 35/53%, 39/57%, and 26/44% identity/similarity to *N. gonorrhoeae* *patA*, *patB*, and *ape1*, respectively.

To investigate the role of OAP in *C. jejuni*, the *patA*, *patB*, and *ape1* homologs, as well as the entire gene cluster, were inactivated by deletion-insertion mutagenesis with the non-polar Km^R cassette (*aphA-3*) from pUC18K-2 lacking a transcriptional termination site (Fig. 1C; supplemental text S1) (47). Complementation was achieved using the pRRC integration vector (48). For complementation, the coding region of each OAP gene plus upstream sequence containing the ribosomal binding site was inserted into the genome of the corresponding mutant at ribosomal intergenic regions along with a Cm^R cassette (the Δ *ape1* complemented strain, designated Δ *ape1*^C, is shown in Fig. 1D as an example). Expression of the wild-type genes at the rRNA site was driven from the promoter of the Cm^R cassette.

Growth rate experiments performed on all mutant strains indicated no significant difference in growth rates in broth cultures up to 36 h (data not shown) with the exception of Δ *ape1*^C, which grew at a slower rate (although this slower growth rate

Role of *C. jejuni* Peptidoglycan O-Acetylation

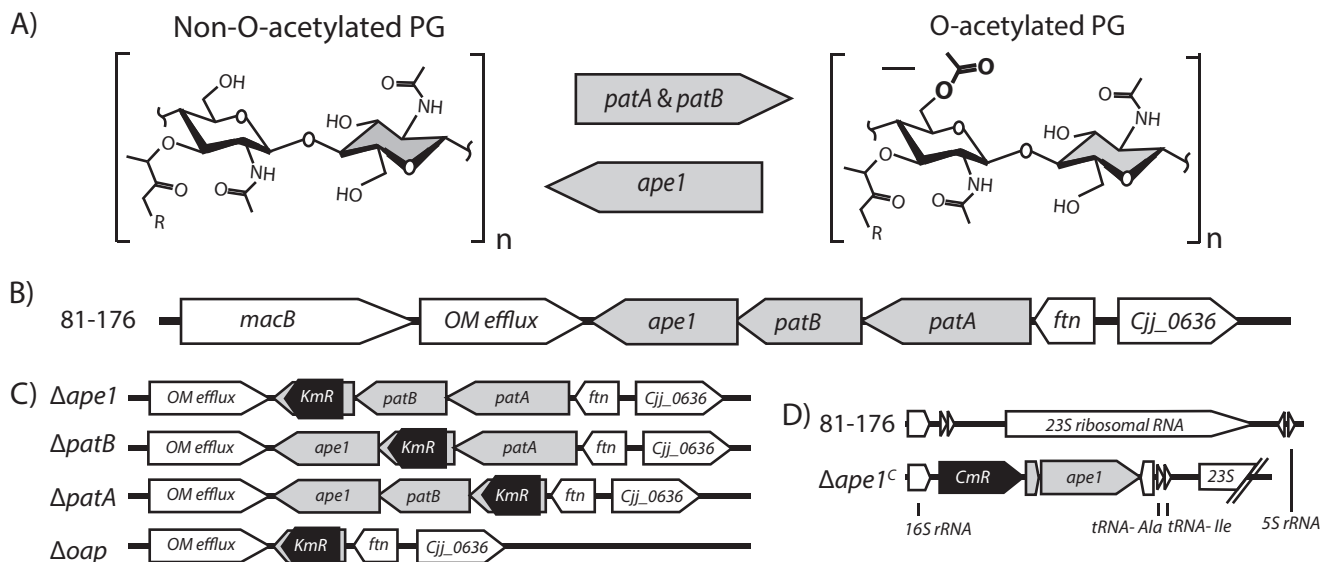


FIGURE 1. Location of O-acetyl groups on peptidoglycan subunits, organization of the *C. jejuni* OAP gene cluster, and description of deletion mutant and complement construction. A, structures of the disaccharide muropeptides showing non-O-acetylated PG and O-acetylated PG, location of O-acetylation (arrow), and the putative involvement of the *oap* genes. B, genomic organization of the *C. jejuni* OAP gene cluster in the 81-176 wild-type strain (gray). *cjj81176_0638*, *cjj81176_0639*, and *cjj81176_0640* are the *C. jejuni* homologs of Δ *ape1*, Δ *patB*, and Δ *patA* respectively, as identified by BLAST using the *N. gonorrhoeae* OAP genes sequences. C, OAP mutants were generated by homologous recombination with a mutated copy of the gene (or the entire cluster for Δ *oap*) in which a portion of the gene (or cluster) was deleted and replaced with a non-polar *Km^R* cassette (*aphA3*) (47). Resistance to *Km* was used as a selective marker for successful homologous recombination in *C. jejuni* with the mutated gene. D, complement construction (with Δ *ape1* used as an example, designated Δ *ape1*^C). Each OAP gene plus upstream sequence containing the ribosomal binding site was cloned into the pRRC vector that contains homologous regions to three ribosomal intergenic regions downstream of the *Cm^R* cassette for selection of successful *C. jejuni* transformants. Complement constructs were transformed into their respective mutant backgrounds. *MacB*, macrolide-specific efflux pump; *OM efflux*, outer membrane efflux; *ftn*, ferritin; 23S, 23S ribosomal RNA (48).

did not affect the ability of Δ *ape1*^C to complement Δ *ape1* phenotypes). Differences were observed in the long term survival properties of Δ *ape1* with more modest differences exhibited by Δ *patA*, Δ *patB*, Δ *oap*, and Δ *ape1*^C. At 48 h, a 1.0-log increase in recovery was observed for Δ *ape1*, but recovery fell at 72 h by 0.8-log relative to wild type. At 48 h, Δ *patA* and Δ *patB* exhibited a 0.3-log increase, and Δ *oap* showed a 0.4-log increase in recovery, relative to wild type. The recovery of all three OAP-deficient mutants was 0.3-log lower than wild type at 72 h. Δ *ape1*^C exhibited a 0.8-log increase in recovery at 48 h and a 0.3-log decrease at 72 h relative to wild type (data not shown).

O-Acetylation Levels of Purified PG from Deletion Mutants Reflect the Putative Functions of the *C. jejuni* OAP Gene Cluster—To determine whether the *C. jejuni* OAP gene homologs were involved in OAP, PG O-acetylation levels were determined for the mutants of the three putative OAP genes (Δ *patA*, Δ *patB*, and Δ *ape1*) and for the mutant lacking the entire cluster (Δ *oap*) (Fig. 1C). PG was isolated from strains using an established protocol that minimizes spontaneous O-linked acetate hydrolysis and was assessed for OAP levels by quantifying released acetate and MurNAc (49, 50).

The O-acetylation level for the wild-type strain 81-176 was determined to be $12.5 \pm 0.71\%$ relative to MurNAc content. O-acetylation levels among the mutants varied according to their predicted function (Table 1). Deletion of *patA* and *patB* resulted in a reduction in O-acetylation levels at 2.45 ± 0.14 and $3.05 \pm 0.22\%$ relative to MurNAc content, respectively. Deletion of the entire gene cluster in Δ *oap* resulted in a decrease in O-acetylation levels to $2.10 \pm 0.18\%$, similar to that of Δ *patA* and Δ *patB*. Previous studies using *Escherichia coli* (which lacks PG O-acetyl groups) showed undetectable levels of acetate

TABLE 1

O-Acetylation levels of *C. jejuni* 81-176, Δ *ape1*, Δ *ape1*^C (complemented Δ *ape1*), Δ *patB*, Δ *patA*, and Δ *oap* (a mutant in which the entire cluster was deleted: *ape1*, *patB*, and *patA*), as determined by base-catalyzed hydrolysis and release of acetate reported as a % O-acetylation relative to MurNAc content

Strain	% O-acetylation ^a (mean \pm S.D.)
81-176	12.5 \pm 0.71
Δ <i>ape1</i>	35.6 \pm 2.25
Δ <i>ape1</i> ^C	11.8 \pm 0.52
Δ <i>patB</i>	3.05 \pm 0.22
Δ <i>patA</i>	2.45 \pm 0.14
Δ <i>oap</i>	2.10 \pm 0.18

^a Results shown are of one representative biological replicate measured in triplicate \pm S.D.

using identical methods (50, 51). This suggests that *patA/B* contributes to PG O-acetylation in *C. jejuni*, but their absence is insufficient to abolish OAP. Deletion of *ape1* led to an increase in O-acetylation to $35.6 \pm 2.25\%$ relative to total MurNAc content. These results are in accordance with the functions described for homologs in *N. gonorrhoeae* and *N. meningitidis* (30, 42–44). O-Acetylation levels were restored to wild-type levels in the Δ *ape1* complement ($11.78 \pm 0.52\%$). Analysis of the O-acetylation levels for Δ *patA* and Δ *patB* complements were not performed as, unlike the Δ *ape1* mutant, phenotypic differences between these mutants, Δ *oap* and wild type, were in almost every case not statistically significant or were minimal (see below).

***C. jejuni* OAP Mutants Exhibit Altered PG Muropeptide Profiles, with Δ *ape1* Displaying the Most Dramatic Changes from Wild Type**—O-Acetylation has been described as a PG maturation event occurring after transglycosylation and transpeptidation (30). Cleavage of PG by bacterial LTs is inhibited by PG O-acetylation. Thus, O-acetylation may impact PG maturation

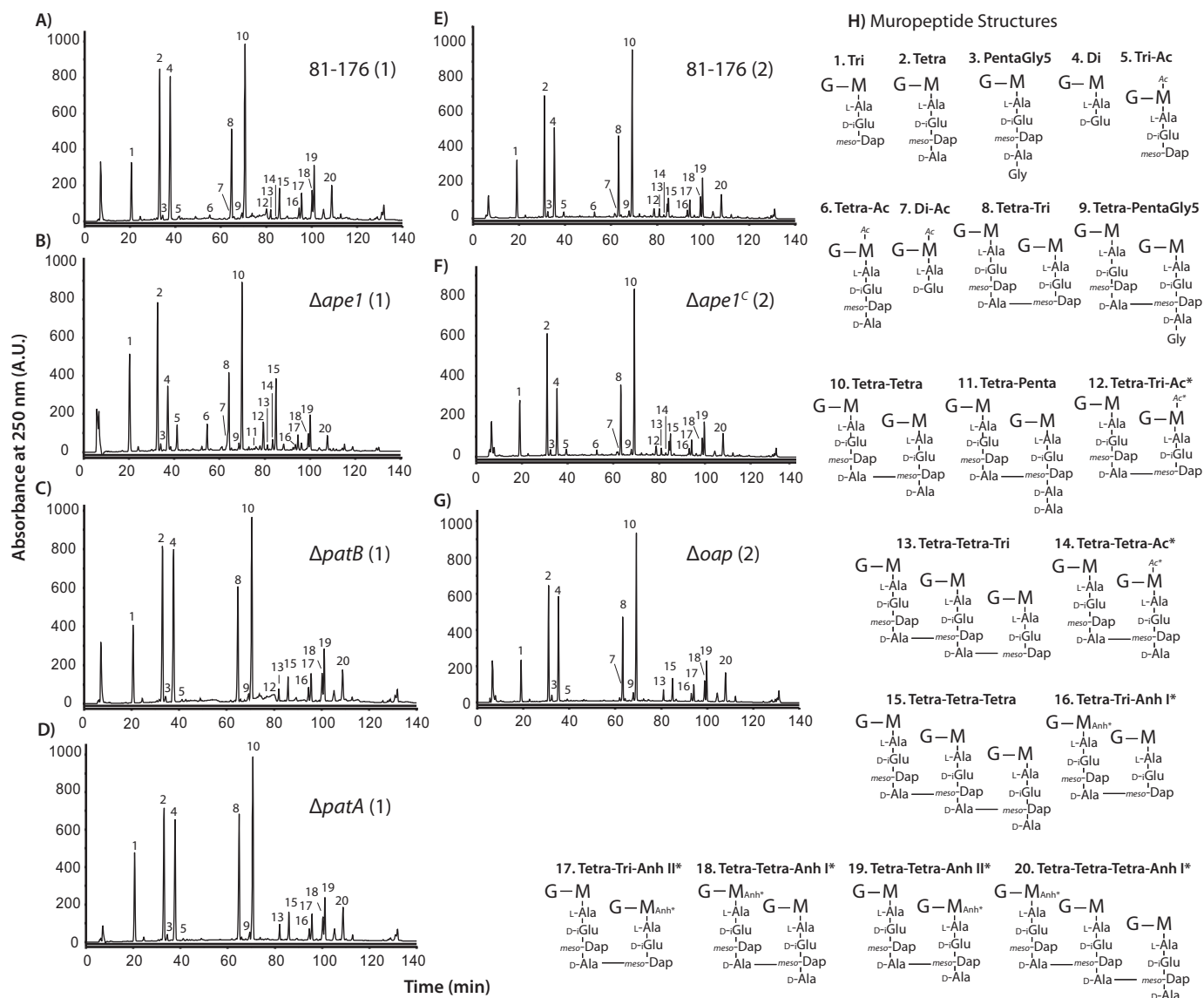


FIGURE 2. HPLC elution profile of *C. jejuni* mucopeptides and proposed mucopeptide structures. Purified PG was digested with cellosyl, and the resulting mucopeptides were reduced with sodium borohydride and separated on a Prontosil 120-3-C18 AQ reverse-phase column. HPLC profiles are shown for wild-type strain 81-176 (A and E), Δ *ape1* (B), Δ *patB* (C), Δ *patA* (D), Δ *ape1*^C (F), and Δ *oap* (G). Mucopeptide profiles were generated in two sets of experiments indicated by (1) for Sample Set 1 and (2) for Sample Set 2. The mucopeptide structure represented by each peak was determined previously by mass spectroscopy (18), and proposed mucopeptide structures of each peak corresponding to the peak number in the chromatogram are shown in H. The summary of the mucopeptide composition is shown in Table 3. G, N-acetylglucosamine; M, reduced N-acetylmuramic acid; L-Ala, L-alanine; D-iGlu, D-isoglutamic acid; meso-Dap, meso-diaminopimelic acid; D-Ala, D-alanine; Ac, O-acetyl groups at MurNAC C6 position; Anh, 1,6-anhydro group of MurNAC; *, it is not known on which MurNAC residue the modification occurs.

events in *C. jejuni*, affecting aspects such as mucopeptide profiles and glycan chain length (52). To investigate this, PG was isolated from wild type and each of the mutant and complemented strains, and the mucopeptide composition was determined. HPLCs are shown in Fig. 2. Raw data (relative abundance of each mucopeptide) and summarized mucopeptide profiles can be found in Tables 2 and 3, respectively.

The method used for mucopeptide analysis results in the loss of some of the PG O-acetyl groups (due to the alkaline conditions for NaBH₄ reduction resulting in base-catalyzed hydrolysis of the O-linked acetate) and is thus less precise at determining O-acetylation levels than the methodology used above. Nonetheless, similar trends were observed, further supporting gene product function. PG O-acetylation levels were reduced in

Δ *patA*, Δ *patB*, and Δ *oap* and increased in Δ *ape1* relative to wild-type 81-176. Monomeric O-acetylated tetrapeptide species and O-acetylated tetra-tetra dimeric species were absent in Δ *patB*, Δ *patA*, and Δ *oap*. The abundance of all detectable O-acetylated mucopeptide species was increased in Δ *ape1*.

Δ *ape1* exhibited a large decrease in total anhMP species and an increased average glycan chain length compared with wild type, similar to observations made in *N. meningitidis* (33), and is consistent with the observed O-acetylation levels, as de-O-acetylation must precede LT activity. Conversely, in the absence of *patA* or *patB*, the relative abundance of anhMP species did not vary strongly from wild type.

Changes were also observed in other mucopeptide species between wild type and Δ *patA*, Δ *patB*, Δ *oap*, and Δ *ape1*. The

Role of *C. jejuni* Peptidoglycan O-Acetylation

TABLE 2

Muropeptide composition of *C. jejuni* wild-type 81-176, Δ *ape1*, Δ *patB*, and Δ *patA*, Δ *ape1*^C, Δ *patB*^C, Δ *patA*^C, and Δ *oap* showing relative abundance of muropeptides corresponding to peaks in HPLCs (Fig. 2)

Peaks ^a	Muropeptide	Sample Set #1				Sample Set #2				
		81-176	Δ <i>ape1</i>	Δ <i>patB</i>	Δ <i>patA</i>	81-176	Δ <i>ape1</i> ^C	Δ <i>patB</i> ^C	Δ <i>patA</i> ^C	Δ <i>oap</i>
1	Tri	5.8	12.3	7.3	9.5	8.8	9.6	8.8	6.0	6.2
^b 2	Tetra-Gly-4					0.4	0.4	0.4	0.3	0.4
3	Tetra	16.1	16.6	15.8	15.2	16.1	16.9	16.2	15.7	15.1
4	Penta-Gly-5	0.6	0.8	0.7	0.7	0.8	1.0	1.2	0.9	1.0
5	Di	16.3	8.3	16.1	14.3	13.0	10.1	10.4	16.2	15.7
6	Tri-Ac	0.3	2.8	0.3	0.3	1.0	1.2	0.7	0.5	0.4
7	Tetra-Ac	0.6	2.6	0.0	0.0	0.6	0.7	0.5	0.0	0.0
8	Di-Ac	0.0	1.9	0.0	0.0	0.2	0.5	0.5	0.6	0.4
9	TetraTri	9.7	7.6	11.1	13.7	10.5	10.1	10.6	11.5	11.2
10	TetraPenta-Gly-5	0.4	0.7	0.6	1.0	0.8	0.9	1.0	0.8	1.2
11	TetraTetra	19.0	17.0	18.0	21.2	21.4	22.4	23.0	22.4	22.5
12	TetraPenta	0.0	0.1	0.0	0.0					
13	TetraTri-Ac	1.8	3.4	1.6	0.0	1.5	1.7	0.9	0.0	0.0
14	TetraTetraTri	0.8	0.5	0.9	1.5	1.0	0.9	1.3	1.3	1.4
15	TetraTetra-Ac	0.3	1.1	0.0	0.0	1.7	1.8	1.4	0.4	0.0
16	TetraTetraTetra	2.9	7.0	1.9	2.8	2.5	2.8	3.1	2.9	3.4
17	TetraTriAnh I	1.2	0.5	1.3	1.3	1.1	1.0	1.1	1.3	1.2
18	TetraTriAnh II	2.6	1.6	2.5	2.7	2.4	2.1	2.2	2.5	2.5
19	TetraTetraAnh I	3.0	1.8	2.8	2.7	2.8	2.8	3.0	3.1	3.0
20	TetraTetraAnh II	5.6	3.7	4.9	4.9	5.2	5.0	5.1	5.4	5.5
^b 20	TetraTetraTriAnh					1.1	0.9	1.3	1.4	1.7
1-20	All known ^c	91.2	92.3	89.5	95.9	96.8	97.1	97.4	97.7	97.9

^a Peak numbers correspond to those from HPLCs in Fig. 2. Muropeptides are named according to Glauner *et al.* (88) and are depicted in Fig. 2H. Di, disaccharide dipeptide (disaccharide = β 1,4-linked *N*-acetylglucosamine-*N*-acetylmuramic acid); Tri, disaccharide tripeptide; Tetra, disaccharide tetrapeptide; Penta, disaccharide pentapeptide. Muropeptides 1-7 are monomeric, and muropeptides 8-20 are dimers and trimers connected by peptide cross-links. Modifications: Gly, glycine in position 5 of a peptide side chain; Ac, *O*-acetyl groups at the C-6 hydroxyl group of MurNAc; Anh, 1,6-anhydro-*N*-acetylmuramic acid.

^b Peak was previously unidentified in Sample Set #1.

^c The total abundance does not add up to 100% due to the presence of peaks for which a structure has not been assigned.

TABLE 3

Summary of PG muropeptide composition for *C. jejuni* 81-176, Δ *ape1*, Δ *patB*, Δ *patA*, Δ *ape1*^C, Δ *patB*^C, Δ *patA*^C, and Δ *oap*

Muropeptide species	Percentage of peak area ^a									
	Sample Set #1				Sample Set #2					
	81-176	Δ <i>ape1</i>	Δ <i>patB</i>	Δ <i>patA</i>	81-176	Δ <i>ape1</i> ^C	Δ <i>patB</i> ^C	Δ <i>patA</i> ^C	Δ <i>oap</i>	
Monomers (total)	43.5	49.1	44.9	41.7	42.2	41.5	39.6	41.2	40.0	
Dipeptide	17.8	11.0*	18.0	15.0	13.6	11.0	11.2	17.2	16.4	
Tripeptide	6.7	16.4*	8.5	10.2*	10.1	11.1	9.7	6.6*	6.7*	
Tetrapeptide	18.3	20.9	17.6	15.8	17.2	18.1	17.1	16.1	15.5	
Pentapeptides-Gly	0.6	0.9*	0.7	0.7	0.8	1.0	1.3*	0.9	1.0	
O-Acetylated	1.0	8.0*	0.3*	0.3*	1.9	2.4	1.7	1.1*	0.8*	
Dimers (total)	47.7	40.7	47.6	49.4	48.8	49.4	49.5	48.5	48.1	
TetraTri	16.8	14.2	18.4	18.5	16.0	15.5	15.2	15.7	15.2	
TetraTetra	30.5	25.6	28.6	29.9	32.0	33.0	33.2	32.0	31.7	
TetraPentaGly	0.4	0.9*	0.6*	1.0*	0.8	0.9	1.1*	0.8	1.2*	
Anhydro-Dimers	13.5	8.2*	12.7	12.1	11.8	11.3	11.6	12.6	12.4	
O-Acetylated	2.2	4.9*	1.7	0*	3.2	3.7	2.3	0.4*	0*	
Trimers (total)	8.8	10.2	7.5	8.8	7.8	8.1	9.5	8.9	10.2*	
TetraTetraTri	0.9	0.5*	1.0	1.5*	1.0	0.9	1.3*	1.3*	1.4*	
TetraTetraTetra	8.0	9.7	6.5	7.3	6.8	7.2	8.2	7.6	8.8	
Dipeptides (total)	17.8	11.0*	18.0	15.0	13.6	11.0	11.2	17.2	16.4	
Tripeptides (total)	15.4	23.6*	18.0	19.9	18.4	19.1	17.7	14.9	14.7	
Tetrapeptides (total)	65.9	64.0	62.9	63.9	65.1	67.1	67.6	64.8	65.1	
Pentapeptides (total)	0.8	1.3*	1.0	1.2*	1.2	1.5	1.9	1.3	1.6*	
O-Acetylated (total)	2.1	10.4*	1.2*	0.3*	3.5	4.3	2.9	1.3*	0.8*	
Anhydromuropeptides	8.3	4.8*	7.8	7.5	7.7	7.4	7.9	8.3	8.6	
Average chain length	12.0	20.8*	12.8	13.3	13.0	13.5	12.6	12.0	11.6	
Degree of cross-linkage	29.7	27.2	28.8	30.6	29.6	30.1	31.1	30.2	30.9	
% peptide cross-links	56.5	50.9	55.1	58.3	57.8	58.5	60.4	58.8	60.0	

^a Values represent the percentage area of each muropeptide from raw data (found in Table 2) calculated to give a total of 100%. Boldface numbers represent a change in relative abundance of $\geq 20\%$ from wild type. Boldface numbers with an asterisk represent $\geq 30\%$ change from wild type. Percentages shown are calculated from values rounded to the nearest 0.1%. Muropeptide profiles were generated in two sets of experiments, Sample Set #1 and Sample Set #2. Muropeptide profiles were compared with the wild-type 81-176 muropeptide profile that was analyzed in the same sample set.

Δ *patA* mutant showed an increase in monomeric tripeptides, tetra-penta dipeptides, and tetra-tetra-tri tripeptides. For Δ *patB*, the monomeric tripeptides and dimeric tetra-penta species increased relative to wild type. Δ *oap* exhibited some differences from wild type that followed the same trend as with

Δ *patA*, an increase in tetra-penta dipeptides and tetra-tetra-tri tripeptides, and some that were unique to Δ *oap*, an increase in dipeptides and a decrease in tripeptides. Analyses of PG muropeptide profiles for Δ *patA*- and Δ *patB*-complemented strains Δ *patA*^C and Δ *patB*^C showed minimal changes from wild type

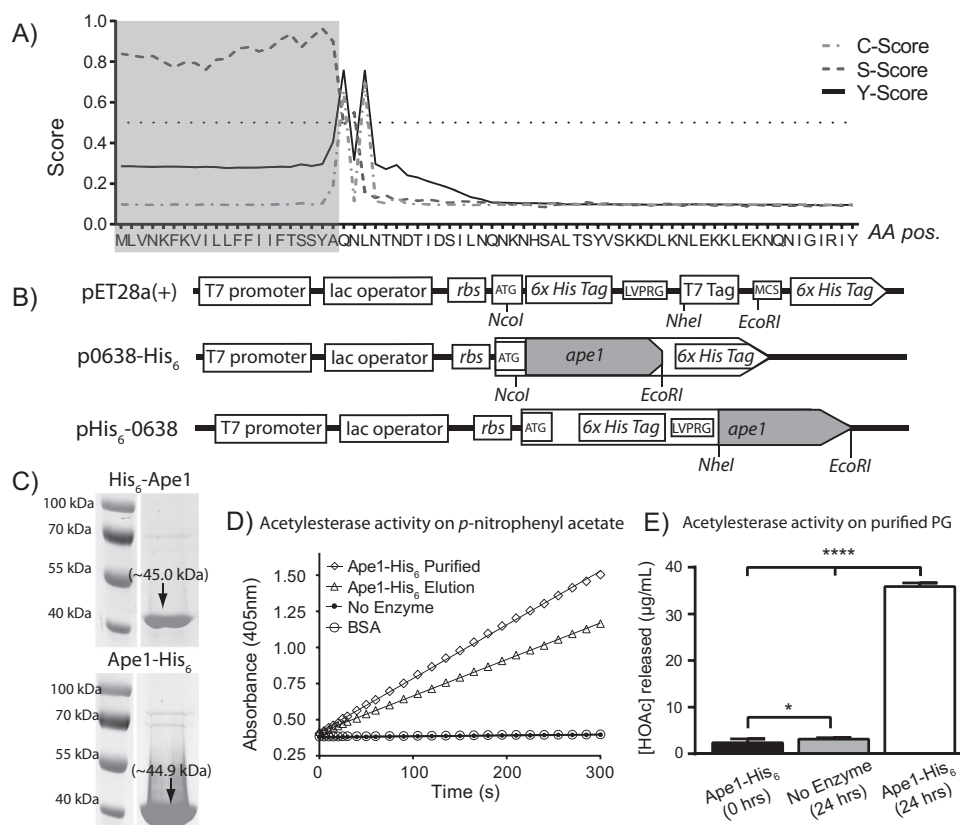


FIGURE 3. A, SignalP 4.1 server (83) output for signal peptide prediction of in-frame translation of *Cjj81-176_0638*. *C*-score (the predicted first amino acid of the mature protein), *S*-score (the likelihood that a particular amino acid is part of a signal peptide), and *Y*-score (amino acid with a high *C*-score exhibiting the greatest change in the *S*-score) predicted the cleavage site to be between the 21st and 22nd amino acids. B, *Cjj81-176_0638* was cloned in-frame without the signal peptide into pET28a(+) protein expression vectors. Top, map of cloning sites in pET28a(+) commercial expression vector. Middle, Ape1-His₆ expression construct. NcoI and EcoRI were used to produce a C-terminal His₆-tagged Ape1 protein that uses ATG start codon and TGA stop codon encoded in the vector. Bottom, His₆-Ape1 expression construct. NheI and EcoRI were used to produce an N-terminal His₆-tagged protein that uses AUG start codon encoded by the vector and the original stop codon from *Cjj81-176_0638*. rbs, ribosome-binding site; LVPRG, thrombin cleavage site; MCS, multiple cloning sites. Gene organization not to scale. C, His₆-tagged Ape1 after nickel-nitrilotriacetic acid-agarose purification shows protein of the predicted size (45.0 and 44.9 kDa for His₆-Ape1 and Ape1-His₆, respectively) in eluted fractions after SDS-PAGE analysis. D, purified Ape1-His₆ exhibits acetyltransferase/deacetylase activity using pNPAC as a substrate (45). Reactions were monitored over 5 min as a change in the absorbance at 405 nm (formation of *p*-nitrophenol) after cleavage of the acetyl group. No enzyme control and BSA control are overlapping and show no acetyltransferase activity. Results shown are from one protein purification experiment. Results are reproducible for each expression and purification experiment, and activity was routinely assessed before performing enzymatic assays on PG. E, Ape1-His₆ has acetyltransferase activity using PG mucopeptides as a substrate. Determination of acetic acid concentration after treatment of Δ ape1 PG with Ape1-His₆ for 24 h was performed using Megazyme acetic acid assay kit. Treatment and no enzyme control were compared with acetic acid concentration at 0 h of treatment using Student's *t* test with * and **** indicating *p* values of <0.05 and <0.0001, respectively. Results are from one representative experiment of two biological replicates performed in triplicate.

with restored *O*-acetylation levels for Δ pat^BC but not Δ pat^AC. The largest number of changes and greatest degree of change occurred in Δ ape1. In Δ ape1, total dipeptide species decreased and total tripeptides and pentapeptides increased relative to wild type. The total amount of dimers also appeared to be slightly lower in Δ ape1. The majority of the mucopeptide changes was restored to near wild-type levels in the Δ ape1 complement strain (Δ ape1^C).

Recombinant Ape1 Has in Vitro Acetyltransferase Activity on *p*-Nitrophenyl Acetate and *O*-Acetylated PG—Based on the mucopeptide data observed for Δ ape1 and phenotypic data shown below, the acetyltransferase activity of Ape1 was confirmed biochemically. Ape1 was expressed with a His₆ tag and minus the signal peptide at either the N or C terminus and purified (Fig. 3, A and B). Both recombinant proteins purified well (Fig. 3C), producing 3 ml of 0.9–1.2 mg/ml protein after dialysis from a starting culture of 100 ml. The expected sizes of the recombinant proteins are 45.0 and 44.9 kDa for His₆-Ape1 and Ape1-His₆, respectively. The specific activity of purified Ape1

was determined using *p*-nitrophenylacetate (*p*NPAC), a common substrate used to test esterase activity (31, 32). Specific activity for Ape1-His₆ ranged between 26.1 and 38.9 μmol/min/mg of protein (Fig. 3D), which was higher than the reported specific activity of ~10.4 μmol/min/mg for *N. gonorrhoeae* Ape1 measured under similar reaction conditions (32). This demonstrates that the recombinant protein exhibits acetyltransferase activity. His₆-Ape1 showed similar specific activity with *p*NPAC (data not shown).

Ape1-His₆ was also assayed for acetyltransferase activity on its native substrate (Fig. 3E), *O*-acetylated PG. PG isolated from Δ ape1 was used as the substrate due to the increased PG *O*-acetylation levels in this strain. Cleavage of *O*-acetyl groups was assessed using a commercial acetic acid assay kit (Megazyme) as an end point experiment. At 0 h, the average acetate concentration in the sample was 2.4 ± 0.3 μg/ml. Incubation of Δ ape1 PG for 24 h in the absence of enzyme resulted in an average acetate concentration of 3.1 ± 0.1 μg/ml, and an average acetate concentration of 35.9 ± 0.7 μg/ml after incubation

Role of *C. jejuni* Peptidoglycan O-Acetylation

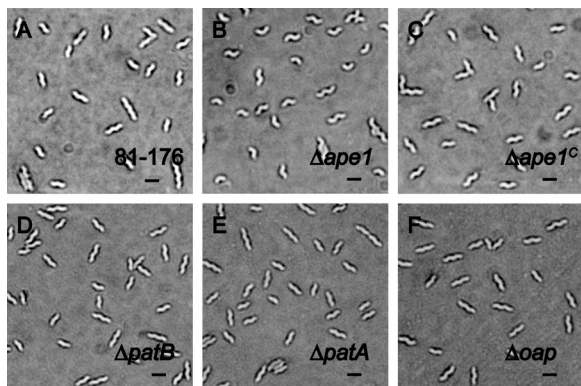


FIGURE 4. *C. jejuni* Δ ape1 mutant has a pleomorphic cell shape, and other OAP mutants display unaltered cell morphology. DICM showing the morphology of wild-type strain *C. jejuni* 81-176 (A), the differentially curved Δ ape1 strain (B), the complemented strain Δ ape1^C with restored morphology (C), Δ patB (D), Δ patA (E), and Δ oap (F). Cells were harvested from 7 h of growth in MH-TV broth at a mid-exponential phase of growth. Scale is 2 μ m (black bar).

with Ape1-His₆. Because of the insoluble nature of PG, data from this assay cannot be expressed in the classical definitions of enzyme kinetics using the native substrate.

Microscopy and CellTool Analyses of *C. jejuni* Δ ape1 Population Morphology Reveal Shape Pleomorphism—Because a number of changes were observed in the muropeptide profiles of the OAP mutants, it was hypothesized that these changes may result in changes in cell shape. The morphology was examined by DICM after 4 and 7 h of growth initiated at an A_{600} of 0.05 to obtain early- and mid-exponential phase cultures (Fig. 4). Whereas wild type exhibited the classical *C. jejuni* helical shape (Fig. 4A), Δ ape1 exhibited primarily “comma-shaped” and differentially curved cells (Fig. 4B). Wild-type helical morphology was restored upon complementation (Fig. 4C). A distinct change in morphology was not observed for the other OAP mutant populations (Fig. 4, D–F).

The open-source shape analysis program CellTool (53) was used to quantify the changes in shape in the OAP mutants (Fig. 5). The program contains a set of tools used to extract shapes from binary images that can then be used to assess and compare the population morphology using a variety of metrics. Extracted shapes from the wild-type population were aligned to one another, and principal component analysis (PCA) was performed to generate a baseline model for variation within the wild-type population. At mid-exponential phase, three shape modes (principal components that define specific changes in cell shape in the population) described 95% of the morphological variation in the *C. jejuni* wild-type population. Each shape mode represented an observable metric (Fig. 5, A and B). Shape mode 1 corresponded to variation in cell length, explaining >90% of the variance (as expected because a population likely exhibits asynchronous growth and division). Shape mode 2 explained 1.9% of the variance and appeared to have some relation to the curvature and wavelength of the cell. A third shape mode explained 1.7% of the variance and described differences in cell width. Contours of mutants were aligned to the wild-type shape model as a reference and Kolmogorov-Smirnov (KS) statistical tests were used to compare sample probability distributions. Based on the large population of bacterial cells assessed

and conditions required for KS analysis, a p value of 0.00001 was used as a cutoff for significance (Fig. 5B) (54).

No strains were significantly different from the wild type in shape mode 1 (cell length) or from each other, with the graphical output also showing that the population distributions overlap very closely. In shape mode 2 (cell curvature), some differences in population distribution between wild type and Δ ape1^C, Δ patA, Δ patB, and Δ oap were significant by the KS cutoff utilized. However, the graphical output showed that these strains were similar to wild type, whereas Δ ape1 exhibited a dramatic shift in the population distribution maximum (~2.2 standard deviations from the wild-type mean). Shape mode 3 (cell width) was significantly different in all strains compared with wild type (with the exception of Δ ape1^C), and each exhibited a shift of approximately 1 S.D. in the population maximum toward a reduced width compared with the wild-type mean as reflected in the graphical output. A 2D scatterplot of measurements of each individual contour of wild type, Δ ape1, and Δ ape1^C populations for shape modes 2 and 3 (Fig. 5C) likewise shows that there was a clear difference in shape for the Δ ape1 population compared with wild type and Δ ape1^C. Early-exponential phase bacteria exhibited similar population shifts as for mid-exponential phase bacteria (with the exception of shape mode 3, as cell width was not captured as a major contributor to the variance in shape for wild type at this time point). The most notable shift at early-exponential phase was observed for cell curvature (shape mode 2) in Δ ape1 (data not shown).

Phenotypic Analyses Reveal the Importance of O-Acetylpeptidoglycan Esterase Activity on Various Aspects of *C. jejuni* Physiology—The OAP mutants were assessed for different phenotypes serving as indicators of transmission and/or colonization efficiency: motility in soft agar, biofilm formation, hydrophobicity, and sensitivity to a variety of inhibitory compounds.

Motility is a major colonization determinant for *C. jejuni* (55). Although all strains exhibited defective halo formation compared with wild type in soft agar plates after point inoculation (Fig. 6A), the halo diameter of Δ ape1 was 70% of wild type, whereas Δ patB, Δ patA, and Δ oap were only modestly defective at 90, 90, and 87% of wild type. Complementation of Δ ape1 restored the halo formation of the mutant to 90% of wild type and was significantly different from that of Δ ape1. In addition, Δ ape1 formed aberrant halos on soft agar with rough perimeters as opposed to the circular halos formed by wild type. This halo phenotype was absent in the other mutants tested and was rescued by complementation.

The ability to form biofilms is important in *C. jejuni* persistence and transmission. *C. jejuni* has been shown to survive up to 28 days in a biofilm state and is a general stress response (56). The ability of our OAP mutants to form biofilms was assessed in borosilicate test tubes by crystal violet staining of standing cultures (57). The Δ ape1 mutant exhibited a hyper-biofilm phenotype, producing 5.5-fold more biofilm than wild type (Fig. 6B). Δ ape1 also developed flocs of bacteria suspended in the broth (58), which were not observed for wild type nor included in the crystal violet quantification of surface-adhered biofilm (data not shown). Complementation of Δ ape1 restored biofilm formation to wild-type levels (Fig. 6B). Biofilms formed

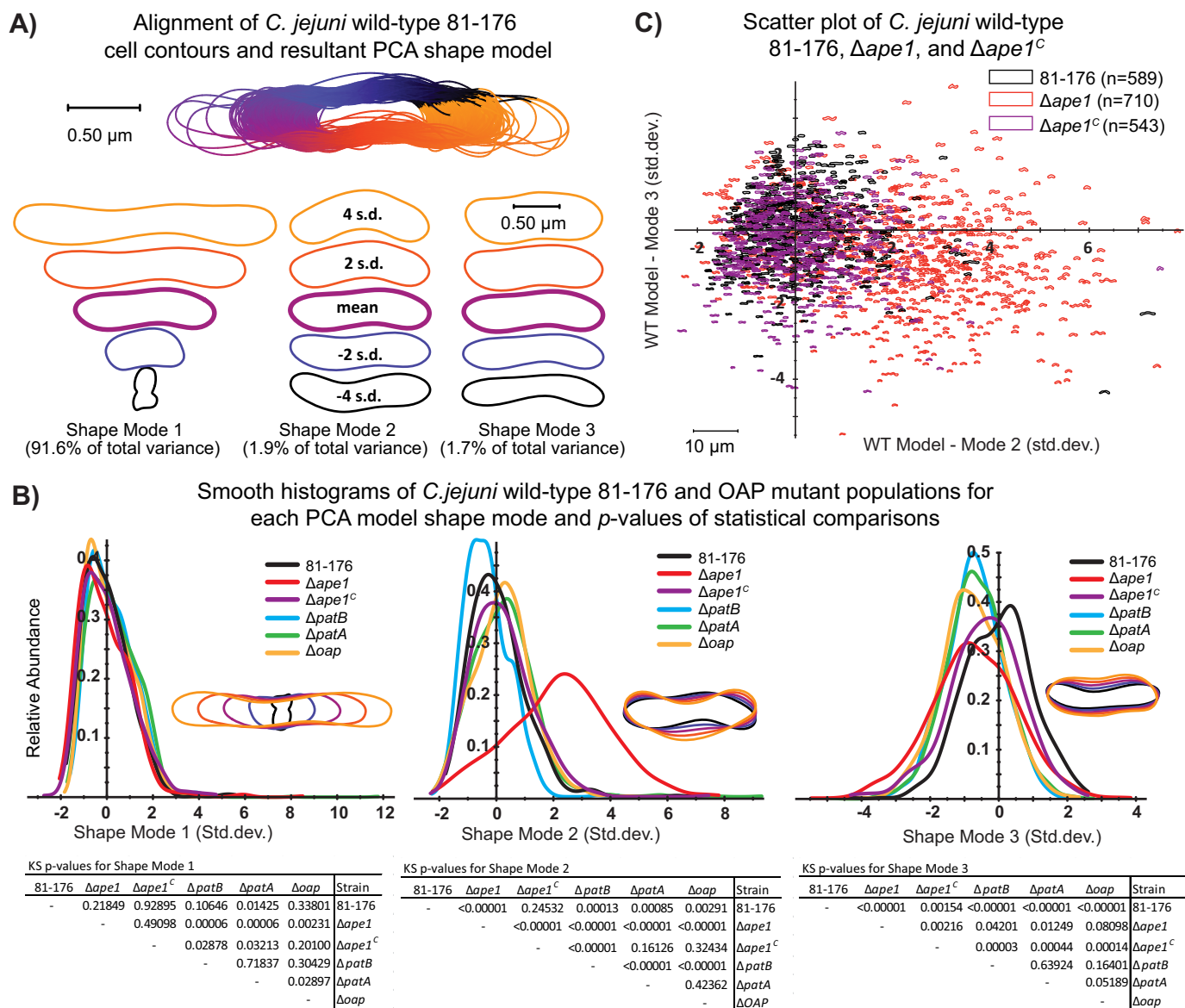


FIGURE 5. CellTool analysis of wild-type strain 81-176, $\Delta ape1$, $\Delta ape1^c$, $\Delta patB$, $\Delta patA$, and Δoap population morphology. Differential interference contrast images were taken of strains grown for 7 h in MH-TV broth at a starting A_{600} of 0.05 (to mid-exponential phase). Images were converted to binary format (white cells on a black background), and lumps and artifacts were manually removed before processing with CellTool “extract contours function” to generate contours representing each cell (53). *A*, contour extraction, alignment, and generation of the PCA shape model for *C. jejuni* wild-type strain 81-176. CellTool “align contours” function was used to align the contours of the wild-type population to one another. *B*, PCA was performed to generate a wild-type shape model that explains 95% variation in the population in principal components called “shape modes.” Shape modes 1, 2, and 3 represent variation in length, curvature/wavelength, and width, respectively. The extracted contours of the mutant populations were then aligned to the wild-type shape model, and a measurement representing the normalized standard deviation from the wild-type mean in each shape mode was generated and depicted graphically. KS tests were performed for each shape mode between each population and are summarized below the plots. *C*, measurements of wild type, $\Delta ape1$, and $\Delta ape1^c$ were plotted with shape mode 2 along the *x* axis and shape mode 3 along the *y* axis to create a scatterplot showing the variation in the different populations.

by $\Delta patB$ and $\Delta patA$ were indistinguishable from wild type, but Δoap produced ~ 2.5 -fold more biofilm than wild type. Characterization of $\Delta ape1$ biofilms by microscopy was unsuccessful as $\Delta ape1$ formed biofilms poorly on coverslips unlike wild type. This indicates altered cell surface properties in $\Delta ape1$. Cell surface hydrophobicity was assessed with hexadecane partitioning (Fig. 6C) (59). The percent hydrophobicity of $\Delta ape1$ was significantly higher (2.0-fold) than wild type and was restored to wild-type levels upon complementation.

The sensitivity of the OAP mutants to detergents, salts, and antimicrobial compounds was tested by determining the mini-

imum inhibitory concentration that reduces growth by 50% relative to a control as measured by A_{600} (MIC_{50}) (Table 4). Only $\Delta ape1$ exhibited an increased susceptibility to any of the compounds tested as follows: the amphipathic bile salt sodium deoxycholate (DOC) and $MgCl_2$. For $\Delta ape1$, an MIC_{50} range for DOC of 0.16 to 0.31 mg/ml was observed, whereas the MIC_{50} for wild type was greater than the highest concentration of DOC tested (> 10 mg/ml). $\Delta ape1$ exhibited a 4–8-fold reduction in MIC_{50} for $MgCl_2$ compared with wild type. Complementation of $\Delta ape1$ restored wild type sensitivity profiles.

Role of *C. jejuni* Peptidoglycan O-Acetylation

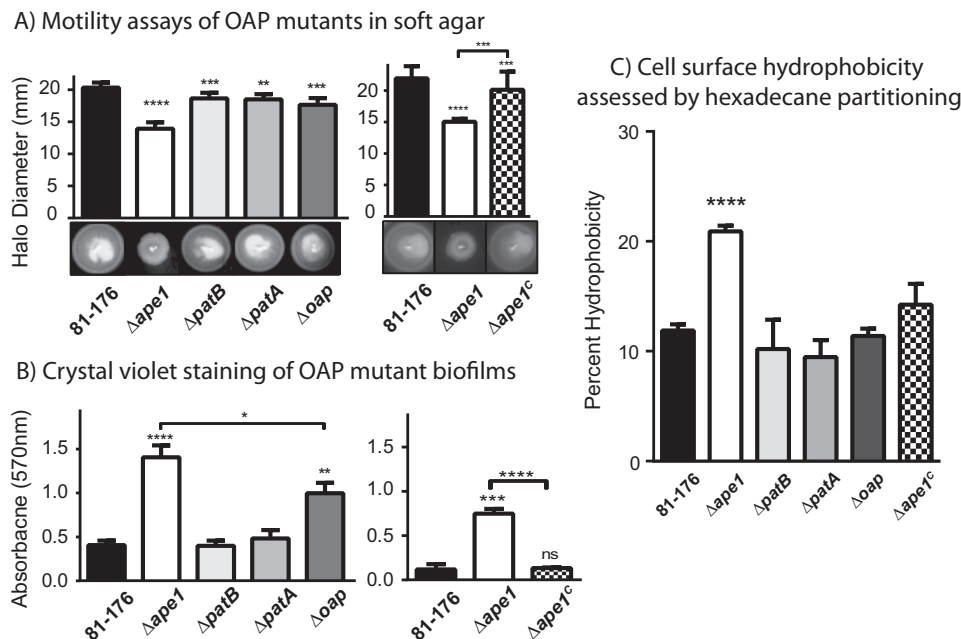


FIGURE 6. Motility in soft agar, biofilm formation, and cell surface hydrophobicity of OAP mutants and wild-type strain 81-176. *A*, $\Delta ape1$ exhibits a 30% decrease in halo diameter and abnormal halo formation (rough edges). Motility in soft agar was assessed by measuring the halo diameter after 24 h of strains point-inoculated in 0.4% semi-solid agar. Representative images of halos are shown *below* each graph. Results shown are representative of one of three independent experiments with 6 replicates. Each strain was compared with wild-type using a paired Student's *t* test, with **, ***, and **** indicating $p < 0.01$, $p < 0.001$, and $p < 0.0001$. *B*, $\Delta ape1$ and Δoap exhibit 5.5- and 2.5-fold enhanced biofilm formation, respectively, at 24 h. Biofilm formation was assessed after 24 h by crystal violet staining of standing cultures in borosilicate tubes and spectrophotometric quantification of dissolved crystal violet at 570 nm. Results shown for the mutants (*left*) are representative of one of three independent experiments carried out in triplicate. The results for $\Delta ape1^c$ (*right*) are representative of one of two experiments performed in triplicate. *ns*, not significant. *C*, $\Delta ape1$ exhibited a 2.0-fold increase hydrophobicity relative to wild type, as assessed by hexadecane partitioning. Results are representative of one of three independent experiments performed in triplicate. For biofilm and hydrophobicity, strains were compared using an unpaired Student's *t* test, with *, **, ***, and **** indicating $p < 0.05$, $p < 0.01$, $p < 0.001$, and $p < 0.0001$. Error bars represent standard deviation.

TABLE 4

MIC₅₀ of *C. jejuni* OAP mutants determined by broth dilution

Measurements indicated with a “-” have not been tested. Measurements in boldface were consistently ≥ 4 -fold different from wild type over three experiments. MIC₅₀, minimum inhibitory concentration to reduce growth by 50% as assessed by optical density.

Compound	MIC ₅₀					
	81-176	$\Delta ape1$	$\Delta patB$	$\Delta patA$	Δoap	$\Delta ape1^c$
Detergents						
Deoxycholate (mg/ml)	>10	0.16–0.31	5->10	1.3->10	1.3->10	1.3->10
SDS (mg/ml)	10–12.5	2.5–6.25	10–12.5	2.5–12.5	5–6.25	12.5
Triton (% v/v)	0.05	0.02–0.005	0.02–0.05	0.02–0.05	0.05	0.05
Antimicrobials						
Ampicillin (μ g/ml)	2.4–4.9	1.2–4.9	4.9	4.9	2.4–4.9	2.4
Lysozyme (mg/ml)	>5	>5	>5	>5	>5	>5
Polymyxin B (μ g/ml)	20	10	10	10	10	10–20
Protamine (μ g/ml)	31.3	15.6–31.3				31.3–62.5
Chelating agent						
EDTA (μ M)	78–156	1.2–156	156	156	156	156
Salts						
NaCl (mM)	62.5–250	31.3–62.5	62.5–125	125	62.5–125	62.5–125
MgCl ₂ (mM)	62.5–125	15.6	62.5–125	62.5–125	62.5–125	62.5–125
CaCl ₂ (mM)	125	125–250	125–250	125–500	500	125
KCl (mM)	62.5	31.3–62.5	62.5	31.3–62.5	125	31.3–62.5

Ape1 Is Required for C. jejuni Bacteria-Host Interactions—The contribution of OAP to *C. jejuni* host interactions was examined by determining recovery of the mutants after chick colonization and host cell infections, as well as the ability to elicit IL-8 secretion *in vitro* in human epithelial infections.

Chickens are an avian reservoir for *C. jejuni* and a common source of human infection. The $\Delta ape1$ mutant exhibited a significant 4.4-log decrease in colonization (Fig. 7A),

whereas $\Delta patB$, $\Delta patA$, and Δoap mutants were not defective for chick colonization. The defects in long term survival in broth for the OAP-deficient mutants were modest compared with $\Delta ape1$, so the defect in chick colonization could be related to the altered long term survival properties of $\Delta ape1$.

The ability of a *C. jejuni* strain to invade and survive in non-phagocytic epithelial cell lines has been shown to correlate with virulence (11, 60, 61). The ability of the *C. jejuni* OAP mutants to

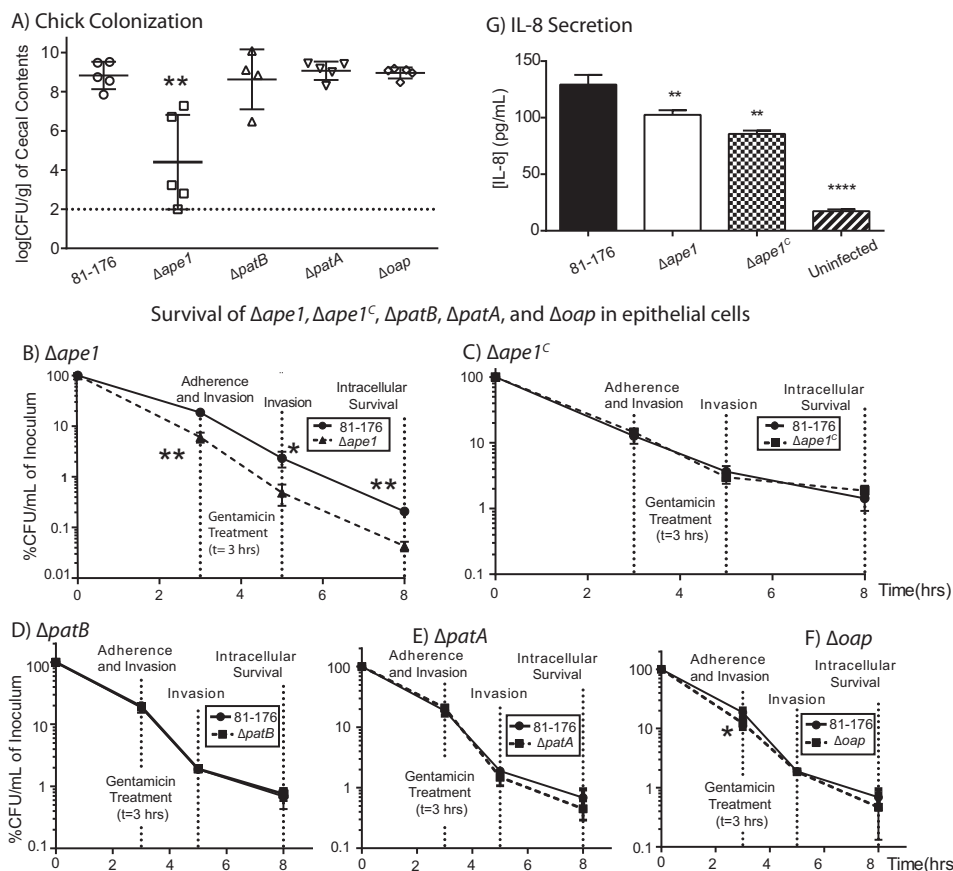


FIGURE 7. Effect of OAP levels on *C. jejuni* host-bacteria interactions. *A*, Δ ape1 shows reduced chick colonization compared with wild-type strain 81-176, whereas Δ patB, Δ patA, and Δ oap mutants display wild-type colonization. Each point represents the recovery of *C. jejuni* strains in log CFU/g of cecal contents from individual day-old chicks 6 days post-colonization with 1×10^4 CFU/ml of the indicated strain. The geometric mean is denoted by a black bar. Error bars represent 95% confidence intervals. Adherence, invasion, and intracellular survival of *C. jejuni* in INT407 epithelial cells were assessed by a Gm protection assay and OAP mutant strains. Δ ape1 (*B*) shows a reduced ability to adhere to, invade, and survive in INT407 epithelial cells that were restored upon complementation (*C*). Δ patB (*D*), Δ patA (*E*), and Δ oap (*F*) exhibit near wild-type adherence, invasion, and intracellular survival properties. INT407 cells were infected with *C. jejuni* at a multiplicity of infection of ~ 80 . Adherence and invasion were quantified at 3 h post-infection. At this point, the media in the remaining wells were replaced with MEM containing gentamicin (150 μ g/ml) and incubated for 2 h, after which the amount of bacterial cells that had invaded the epithelial cells was measured (5-h invasion time point). The Gm in the remaining wells was washed off, and the cells were incubated with fresh MEM containing 3% FBS and a low dose of Gm (10 μ g/ml) for an additional 3 h (8-h intracellular survival time point). CFU/ml was determined for each well by lysing the cells with water and plating the dilutions onto MH-TV plates. Results for *B* and *C* are representative of three independent experiments performed in biological triplicate. The data in *D*, *E*, and *F* are representative of two independent experiments performed with three biological replicates. *G*, INT407 epithelial cells secrete less IL-8 upon infection with Δ ape1 than wild type. Results are from one representative experiment of three independent experiments performed in triplicate. Error bars represent the standard deviation. *, denotes statistically significant difference using the unpaired Student's *t* test, with *, **, and **** indicating $p < 0.05$, $p < 0.01$, and $p < 0.00001$ respectively.

adhere to, invade, and survive inside the human epithelial cell line INT407 was assessed by a gentamicin (Gm) protection assay. Recovery of Δ ape1 was significantly reduced at the adherence, invasion, and intracellular survival time points in comparison with wild type (Fig. 7*B*). Δ ape1^C, Δ patB, Δ patA, and Δ oap displayed wild-type INT407 infection profiles (Fig. 7, *C–F*).

As Δ ape1 was the only OAP mutant to demonstrate reduced invasion of the INT407 cells, its ability to elicit IL-8 secretion from INT407 cells was assessed by ELISA. Cells infected with Δ ape1 reproducibly exhibited statistically significant lower levels (60–79%) of IL-8 secretion compared with cells infected with wild type (Fig. 7*G*). Δ ape1^C did not complement IL-8 induction defects.

Discussion

PG plays roles in multiple facets of bacterial physiology. PG modifications have been shown to influence pathogenic properties in several bacterial species (15, 20, 36). Here, the OAP genes in *C. jejuni* were shown to contribute to PG O-acetyla-

tion/de-O-acetylation, consistent with their predicted functions. These genes were also important for several key physiological and pathogenic properties. This was most notable for *ape1*, which was involved in PG de-O-acetylation and the only OAP gene significantly required for every phenotype examined.

Deletion of *patA* or *patB*, which act to O-acetylate MurNAC, was non-lethal as found in several other bacterial species (33, 37, 44). This suggests that O-acetyl groups added by PatA/B play a non-essential role for growth of *C. jejuni* in the laboratory. Unlike in *N. meningitidis* where OAP is exclusively mediated by *patA/B* (33), the O-acetylation levels were not reduced to 0% in *C. jejuni*, indicating the presence of alternative PG O-acetylation machinery or compensation by alternative mechanisms, as was observed with *E. coli* WechI that acted as an acetate transporter (62). Expression of *N. gonorrhoeae* PatB in *E. coli* increased OAP levels from <0.05 to 1%, which was detrimental to the cells (62). The effect of low levels of OAP on *E. coli* biology provides support that the residual O-acetylation

Role of *C. jejuni* Peptidoglycan O-Acetylation

in *C. jejuni* may be sufficient to mask mutant phenotypes in $\Delta patA/B/oap$ that would otherwise be observed if PG O-acetylation were completely absent. There are conflicting results for the essentiality of *ape1* in *N. gonorrhoeae* (43, 44). In *C. jejuni*, *ape1* was not essential. Deletion of *ape1* resulted in increased O-acetylation levels almost triple that of wild type, supporting the role of Ape1 in *C. jejuni* PG de-O-acetylation. Ape1 acetyltransferase activity was also confirmed *in vitro* using the artificial substrate pNPAC as well as its natural substrate, O-acetylated PG from $\Delta ape1$.

It should be noted that the OAP levels of wild-type *C. jejuni* 81-176 described here were lower than those reported in a previous study for ATCC 700819 and NCTC 11168 (42). However, the strains and growth conditions used differed between the studies. A direct comparison of how these and other potential factors might affect *C. jejuni* PG O-acetylation has not yet been assessed but will be the topic of future work.

As with the OAP analyses described above, the muropeptide profiles also showed differences in PG O-acetylation levels for the *C. jejuni* OAP mutants. Although these data are not truly quantitative for O-acetylation, they offer additional qualitative support for the role of these OAP genes in PG O-acetylation. *N. meningitidis* $\Delta ape1$ showed an increase in only O-acetylated muropeptides with a tri-peptide stem in comparison with wild type (33), although the muropeptide analysis of *C. jejuni* $\Delta ape1$ suggests that Ape1 in *C. jejuni* may be regulated differently, as this specificity was not observed. Previous observations with *N. gonorrhoeae* PatB O-acetyltransferase using *in vitro* assays showed specificity of PatB toward O-acetylation of tetrapeptides (30). A decrease in O-acetylated tetrapeptide species was observed for the *C. jejuni* $\Delta patA$ and $\Delta patB$ mutants (Table 2); however, as this could have been due to hydrolysis during the preparation procedure, further biochemical analysis will be required.

As expected, $\Delta ape1$ also exhibited a 42.1% decrease in relative anhMP levels (presumably due to impaired LT activity) and a greater average chain length. Although chain length was not directly measured, these data support previous findings that Ape1 regulates PG chain length as in *N. meningitidis* (33). The anhMP levels changed only marginally in $\Delta patA$, $\Delta patB$, and Δoap supporting a putative compensation of O-acetylation by a yet unknown mechanism consistent with our OAP analyses and/or O-acetylation itself may not be an essential or the only control mechanism for LT activity in *C. jejuni*. LTs in *E. coli* and *Pseudomonas aeruginosa* have been found in complexes with peripheral membrane-bound lipoproteins and PBPs and are thought to be controlled spatially as well as coupled with synthesis to prevent autolysis (52, 63–65). For *C. jejuni*, the observations here do suggest a role for OAP in regulating LT activity, but other control mechanisms likely exist.

Differences in the muropeptide composition could be possible if O-acetyl groups influence substrate recognition by PG remodeling enzymes. Care must be taken in interpreting how differences in relative abundance actually affect overall PG composition. For instance, small changes in muropeptides of low abundance can result in changes $\geq 20\%$ (*i.e.* total penta-Gly-5 species, which were 0.8% in wild type and 1.3% for $\Delta ape1$; Table 3). Conversely, larger changes in muropeptides of high abundance can produce changes $< 20\%$ yet may still be consid-

ered significant. For example, dimeric species constituted 47.7% of the muropeptides in wild type and 40.7% in $\Delta ape1$; this degree of change may be meaningful, as it affects 7% of the total muropeptides, is unique compared with other mutants tested, and would be considered significant using the 10% cutoff described for *H. pylori* (27). Regardless, it is clear that the absence of *ape1* affects the PG muropeptide profile more so than the absence of *patA/B* (Table 3 and Fig. 2). These changes could be a result of increased O-acetylation affecting substrate recognition by PG remodeling enzymes or missing protein-protein interactions in the absence of Ape1 and will require more extensive analysis in later studies.

N. meningitidis Ape1 showed preference for O-acetylated tripeptide substrates *in vivo* (33), as mentioned above. The crystal structure for *N. meningitidis* Ape1 has recently been solved (46), confirming its classification as a member of the Ser-Gly-Asn-His (SGNH) hydrolase superfamily based on active site catalytic residues (32). These residues are also conserved in *C. jejuni* Ape1. The putative PG binding domain in the N-terminal lobe of *N. meningitidis* Ape1 and its interaction with PG have yet to be described (46). As *N. meningitidis* Ape1 was active against various O-acetylated muropeptides *in vitro*, specificity may be due to regulation of activity through unknown interaction partners. The putative PG binding domain at the N terminus may confer substrate specificity (33). There is only 26/42% amino acid sequence identity/similarity between the N-terminal domains of *N. meningitidis* Ape1 and *C. jejuni* Ape1, so the two enzymes may possess different regulatory regions. Another possibility is that *C. jejuni* lacks the Ape1 interaction partners present in *N. meningitidis* conferring substrate specificity.

One of *C. jejuni*'s defining characteristics is its helical shape, a trait defined by the cytoskeleton-like components that coordinate the PG biosynthetic machinery (66). The muropeptide composition was altered in *C. jejuni*/*H. pylori* periplasmic PG hydrolase mutants, *i.e.* $\Delta pgp1/\Delta csd4$ and $\Delta pgp2/\Delta csd6$, and exhibited a straight rod *versus* helical morphology (18, 19, 28, 67). Deletion of *C. jejuni* *ape1* also resulted in altered muropeptide composition and shape, but the change in shape was not as dramatic as in the abovementioned straight-rod mutants. Thus, CellTool was employed for shape quantification. This analysis showed that $\Delta ape1$ was significantly different from the wild-type population in curvature in that it had both an average shape with a larger wavelength compared with wild type and a greater variance of curvature within the population. Ape1 was shown to affect cell size in *N. meningitidis* (33). In this study, there was a significant increase in total area of $\Delta ape1$ cells when compared with wild type at early-exponential phase but not at mid-exponential phase (data not shown). One explanation could be that Ape1 activity varies at different growth stages in *C. jejuni*.

Multiprotein flagellar complexes span the PG layer with some proteins of the complex proposed to directly interact with PG. These proteins include FlgI, which makes up the P-ring of the periplasmic rod-structure in the hook-basal body (55, 68, 69), and MotB in *H. pylori* that makes up part of the flagellar stator responsible for generating torque (70). In *Salmonella enterica*, the switch protein FlgG of the C-ring, which acts as the rotary component of the flagella, responds to chemotactic sig-

nals and interacts with MotA of the stator that in turn interacts with PG-bound MotB (71). In *E. coli*, CheY is the response regulator that interacts with FliG to alter rotational direction of the flagella (72). Homologs of all these flagellar components are found in *C. jejuni* (55).

In *H. pylori*, the loss of the membrane-bound LT, MltD, affected motility without affecting the localization or number of flagella; this was hypothesized to result from the inability of MotA/B to generate torque due to impaired PG-MotB interactions (75). Similarly, the accumulation of O-acetylation in Δ *ape1* and the subsequent effect on LT activity could affect motility. An improperly assembled or unstable stator may impair the ability of the flagella to alter rotational direction in response to chemotactic signals. Mutants in *C. jejuni cheY* appear completely immotile on soft agar but not by microscopy (73, 74). Thus, the halo morphology does not support a complete loss in the ability to alter rotational direction but may still suggest an impaired response. The Δ *pgp1* and Δ *pgp2* straight mutants were also defective for motility in soft agar, so the changes in Δ *ape1* morphology could also account for the observed defects.

Biofilm formation in *C. jejuni* requires flagellum-mediated motility and attachment to a surface, lysis, and release of extracellular DNA to form the biofilm matrix (76). Δ *ape1* was defective for motility in soft agar but was not immotile. Despite this, Δ *ape1* exhibited a hyper- rather than hypo-biofilm formation phenotype. Envelope stress was recently shown to be a trigger for *C. jejuni* biofilm formation. A mutant exhibiting envelope stress was hyper-biofilm, and with DOC at 0.5 mg/ml, *C. jejuni* 81-176 wild type also exhibited enhanced biofilm formation (76). In this study, DOC concentrations below 0.5 mg/ml inhibit growth of Δ *ape1* (MIC₅₀; Table 4). This, together with the hyper-biofilm phenotype and increased cell surface hydrophobicity, suggests that the accumulation of OAP results in altered membrane properties and may be contributing to membrane stress in Δ *ape1*. However, because Δ *oap* exhibited hyper-biofilm formation as well and did not show evidence of membrane stress (*i.e.* no change in surface hydrophobicity or DOC sensitivity), the hyper-biofilm property may be partially independent of Ape1 activity and could be due to the loss of the Ape1 protein itself.

In *E. coli*, PG-associated lipoprotein (Pal) is often found in PG-protein complexes that are proposed to maintain envelope integrity. The phenotypes of some *E. coli pal* deletion mutants share similarities to *C. jejuni* Δ *ape1*, including increased sensitivity to bile salts and signs of altered motility (77). In addition, the PG binding domain of *E. coli* MotB and *E. coli* Pal are interchangeable (78) and both interact with MurNAc; our observations in Δ *ape1* could be a result of the presence of excess of O-acetyl groups on the PG MurNAc residues preventing stabilizing interactions between multiprotein structures and the PG sacculus.

Given the proposed role of O-acetylation in lysozyme resistance, it was expected that *C. jejuni* OAP mutants would demonstrate differential resistance to lysozyme. However, no differences were observed in lysozyme sensitivity (MIC₅₀). Attempts to destabilize the outer membrane by adding EDTA (at MIC₅₀ and concentrations down to 4-fold less than MIC₅₀) or lacto-

ferrin (at physiological concentration of 3 mg/ml, as described previously (37)) to the lysozyme incubations also failed to result in differential lysozyme sensitivity (data not shown). Lysozyme turbidometric assays were also unsuccessful due to the low yield of PG, resulting in an initial absorbance reading too low to accurately detect a response (data not shown).

Chick colonization by Δ *ape1* was significantly impaired compared with wild type and Δ *patA*, Δ *patB*, and Δ *oap* colonized to wild-type levels (Fig. 6A). Motility and chemotaxis are important for colonization (79); thus, this could be a potential explanation for the Δ *ape1* chick data. Alternatively, and/or additionally, the altered morphology and PG structure (18, 19), increased DOC susceptibility, differential long term survival properties, and other as-yet unknown factors could also contribute to the Δ *ape1* colonization defect.

Of the OAP mutants, only Δ *ape1* was impaired in adherence, invasion, and intracellular survival in INT407 epithelial cells. Whether these observations represent defects at each time point, defects in adherence that in turn affect recovery at later time points, or if Δ *ape1* is very rapidly killed upon invasion (as the 3-h “adherence” time point will also reflect invaded bacteria) will require further experimentation. Infection of human INT407 epithelial cells by Δ *ape1* also led to a decrease in IL-8 secretion. This may correlate with its reduced invasion properties.

Somewhat surprisingly, the reduction in PG O-acetylation had no significant effects on colonization, host cell interactions, or any other phenotype examined except for marginal decreases in halo formation, suggesting that under these conditions OAP by PatA and PatB offers no fitness advantage in host survival, which is perplexing and leaves the role of PG O-acetylation in *C. jejuni* yet to be determined. In contrast, the increase in O-acetylated PG in Δ *ape1* was detrimental to *C. jejuni* in multiple aspects important for pathogenesis. Future studies will focus on finding a direct link between PG O-acetylation and the observed changes in physiology, identifying other potential mechanisms of PG O-acetylation and de-O-acetylation, and revealing the underlying cause(s) of the impaired host interactions for Δ *ape1*.

Experimental Procedures

Strains and Growth Conditions—A list of bacterial strains and plasmids used in this study can be found in Table 5. Construction of mutant and complemented strains is described in [supplemental text S1](#) using primers listed in [supplemental Table S1](#). *C. jejuni* strains, unless otherwise stated, were grown in Mueller-Hinton (MH; Oxoid) broth or agar (1.7% w/v) supplemented with vancomycin (10 μg/ml) and trimethoprim (5 μg/ml) and when appropriate kanamycin (Km; 50 μg/ml) and chloramphenicol (Cm; 25 μg/ml). Standard laboratory conditions for *C. jejuni* growth were 38 °C under microaerophilic conditions (12% CO₂, 6% O₂, in N₂) in a Sanyo tri-gas incubator for MH agar or for standing MH broth cultures. For shaking MH broth cultures (hereafter referred to as broth cultures), *C. jejuni* were cultured in airtight jars using the Oxoid CampyGen Atmosphere generation system with shaking at 200 rpm. Experiments were performed using cultures initiated at A₆₀₀ 0.002 and grown in shaking broth for 16–18 h to reach exponential phase. For plasmid construction and protein purifica-

Role of *C. jejuni* Peptidoglycan O-Acetylation

TABLE 5
Bacterial strains or plasmids used in this study

Strain or plasmid	Genotype or description	Source
<i>C. jejuni</i> strains		
81-176	Wild-type isolated from diarrheic patient	87
Δ <i>ape1</i>	81-176 <i>ape1::aphA3;Km^R</i>	This study
Δ <i>patB</i>	81-176 <i>patB::aphA3;Km^R</i>	This study
Δ <i>patA</i>	81-176 <i>patA::aphA3;Km^R</i>	This study
Δ <i>oap</i>	81-176 <i>oap::aphA3;Km^R</i>	This study
Δ <i>ape1^C</i>	81-176 Δ <i>ape1 rrr::ape1</i> (from pRRC-0638)	This study
Δ <i>patB^C</i>	81-176 Δ <i>patB rrr::patB</i> (from pRRC-0639)	This study
Δ <i>patA^C</i>	81-176 Δ <i>patA rrr::patA</i> (from pRRC-0640)	This study
<i>E. coli</i> strains		
DH5- α	F ⁻ , ϕ 80d <i>deoR lacZΔM15 endA1 recA1 hsdR17(r_K-m_K+) supE44 thi-1 gyrA96 relA1 Δ(lacZYA-argF) U169</i>	Invitrogen
BL21(λ DE3)	F ⁻ <i>ompT hsdS_B(r_B⁻, m_B⁻) gal dcm</i> [λ DE3]	Novagen
Plasmids		
pGEM-T	High copy, linearized, T-tailed, Blue/White, Ap ^R	Promega
pUC18-K2	Source of non-polar <i>aphA3</i> cassette; Ap ^R Km ^R	47
pGEM-T-0638	pGEM-T ligated to 0638 amplified with 0637-2 and 0639-5 (2113 bp); Ap ^R	This study
pGEM-0638:: <i>aphA-3</i>	pGEM-T-0638 inverse PCR amplified with 0638-3 and 0638-2 (4098 bp) and ligated to <i>aphA-3</i> (KpnI, HincII); Ap ^R , Km ^R	This study
pGEM-T-0639	pGEM-T ligated to 0639 amplified with 0639-1 and 0639-2 (2146 bp); Ap ^R	This study
pGEM-0639:: <i>aphA-3</i>	pGEM-T-0639 inverse PCR amplified with 0639-3 and 0639-4 (4267 bp) and ligated to <i>aphA-3</i> (KpnI, HincII); Ap ^R , Km ^R	This study
pGEM-T-0640	pGEM-T ligated to 0640 amplified with 0639-6 and 0641-4 (2396 bp); Ap ^R	This study
pGEM-0640:: <i>aphA-3</i>	pGEM-T-0640 inverse PCR amplified with 0640-1 and 0640-2 (4168 bp) and ligated to <i>aphA-3</i> (KpnI, HincII); Ap ^R , Km ^R	This study
pGEM-0638-40:: <i>aphA-3</i>	pGEM-T ligated to 0637 fragment amplified with 0637-1 and 0638-1 (1483 bp), 0641 fragment amplified with 0641-1 and 0641-2 (822 bp), and <i>aphA-3</i> (KpnI, HincII); Ap ^R , Km ^R	This study
pRRC	<i>C. jejuni</i> rRNA spacer integration vector; Cm ^R	48
pRRC-0638	pRRC ligated to 0638 amplified with 0638-C1(NheI) and 0638-C2(MfeI) (1347 bp); Cm ^R	This study
pRRC-0639	pRRC ligated to 0639 amplified with 0639-C1(NheI) and 0639-C2(MfeI) (1276 bp); Cm ^R	This study
pRRC-0640	pRRC ligated to 0640 amplified with 0640-C1(NheI) and 0640-C2(MfeI) (1616 bp); Cm ^R	This study
pET28a(+)	Commercial vector for expression of recombinant His ₆ -tagged protein	Novagen
p0638-His ₆	pET28a(+) ligated to <i>ape1</i> amplified with 0638-eCF (NcoI) and 0638-eCR (EcoRI) (1121 bp) for expression of C-terminal His ₆ -tagged 0638; Km ^R	This study
pHis ₆ -0638	pET28a(+) ligated to <i>ape1</i> amplified with 0638-eNF (NheI) and 0638-eNR (EcoRI) (1116 bp); for expression of N-terminal His ₆ -tagged 0638 Km ^R	This study

tion, *E. coli* (DH5- α or BL21) strains were grown at 37 °C in Luria-Bertani (LB; Sigma) broth or LB agar (7.5% w/v) supplemented with ampicillin (100 μ g/ml), Km (25 μ g/ml), or Cm (15 μ g/ml) as required.

PG Isolation and Assessment of O-Acetylation Levels—PG isolation for O-acetylation analysis was performed as described previously with minor modifications (32, 51). Each strain was grown on ~60 MH-T agar plates (supplemented with Km or Cm as necessary) for ~18–20 h. The cells were harvested from the plate with 1 ml of ice-cold MH broth per plate and added to a conical tube. Strains were assessed by DICM to examine for contamination and the presence of coccoid cells, ensuring that the cultures had not entered stationary phase. *C. jejuni* cells transition from a helical to coccoid form in stationary phase. The cells were collected by centrifugation, resuspended in 50 ml of 25 mM sodium phosphate buffer, pH 6.5, and boiled in an equal volume of 8% w/v SDS in 25 mM sodium phosphate buffered at pH ~6.5 for 3 h under reflux with stirring (final concentration 4% SDS w/v). SDS-insoluble PG was washed with sterile double distilled H₂O (methylene blue/chloroform tests were performed to detect SDS) (80), frozen, and lyophilized. Lyophilized PG was resuspended in a minimal volume of buffer containing 10 mM Tris-HCl, pH 6.5, and 10 mM NaCl and sonicated (Misonix XL 2020, Mandel Scientific) on ice with a microtip for 2 min. The suspension was treated with 100 μ g/ml α -amylase (Fluka Biochemika), 10 μ g/ml DNase I (Invitrogen), 50 μ g/ml RNase A (ThermoScientific), and 20 mM MgSO₄ overnight at 37 °C. Protease (from *Streptomyces griseus*, Sigma), pre-incu-

bated at 60 °C for 2 h, was added to 200 μ g/ml and incubated overnight at 37 °C. Samples were then re-extracted in SDS, purified as above, lyophilized, and stored at -20 °C. O-Acetylation levels of lyophilized PG were evaluated as a ratio of total saponified O-linked acetate relative to total MurNAc content using mild base-catalyzed release of O-linked acetate (0.1 M NaOH, 40 °C for 4 h) and acid-catalyzed hydrolysis (6 N HCl, 100 °C for 1.5 h) for the complete liberation of PG monosaccharides, acetate, and muramic acid content. Components were quantified by HPLC as described previously (49, 50).

PG Isolation and Muropeptide Analysis—Each strain was grown on ~20–25 MH-T plates (supplemented with Km as required) for ~18–20 h to standardize growth phase and harvested with ice-cold MH-TV broth. Strains were assessed by DICM for contamination and coccoid cells to ensure that cultures had not grown into stationary phase. Cells were lysed using the boiling SDS technique as described previously (19). PG was further purified from the cell lysate and digested with the muramidase cellosyl (kindly provided by Hoechst, Frankfurt, Germany). The muropeptides were reduced with sodium borohydride, and subsequently separated by HPLC, all as described previously (81). Muropeptide structures were assigned based on (i) comparison with retention times of known muropeptides from *C. jejuni* and (ii) by mass spectrometry (Fig. 2) (18, 19, 82).

Expression, Purification, and Biochemical Assays of *C. jejuni* *Ape1*-His₆-Cjj81176_0638 (encoding *ape1*) was PCR-amplified without the predicted 21-amino acid signal peptide (as

identified by SignalP 4.1 Server) (83) and cloned into the pET28a(+) (Novagen) expression vector in-frame with the encoded His₆ tag at either the N or C termini of the gene forming pHis₆-0638 and p0638-His₆, respectively (Fig. 3, A and B). Expression constructs were transformed into *E. coli* BL21(ΔDE3), selected for Km^R, and confirmed by PCR and sequencing. Expression and isolation of recombinant Ape1 are described in the supplemental text S2.

Acetyltransferase activity was determined using pNPAC as a colorimetric substrate, as described previously (45). Assays were performed with 2.5 μg/ml purified Ape1-His₆ in 50 mM sodium phosphate buffer, pH 6.5, and 2 mM pNPAC. Reactions were monitored over 5 min, and specific activity was calculated with an experimentally determined molar absorptivity of 3.42 mM⁻¹ cm⁻¹ for *p*-nitrophenol (room temperature at pH 6.5).

PG-*O*-acetyltransferase activity was tested using purified PG retaining *O*-acetyl groups (as described under "PG Isolation and Assessment of *O*-Acetylation Levels"). Lyophilized PG was resuspended in sodium phosphate buffer, pH 6.5, to a concentration of 5 mg/ml and sonicated on ice with a microtip for 2 min (10 s on/10 s off). 500 μl of PG suspension was aliquoted into Eppendorf tubes to which, Ape1-His₆ was added to a concentration of 10 μg/ml (buffer only for negative control). Samples were incubated at 37 °C in a water bath for 24 h, after which samples were centrifuged (10 000 × *g*, 10 min, 4 °C) to pellet PG. Acetate content in supernatants were assessed using a commercial acetic acid assay kit (Megazyme International) as directed by the manufacturer.

Microscopy and CellTool Shape Analysis—Overnight MH-TV log-phase broth cultures were standardized to A₆₀₀ 0.05 and incubated for 4 or 7 h at 38 °C to generate early-exponential phase and mid-exponential phase cultures, respectively. The samples were processed for DICM. Live cells were imaged on agarose slabs on a Nikon Eclipse TE2000-U microscope equipped with a Hamamatsu C4742-95 digital camera.

For CellTool analysis (53), DICM images from multiple fields (yielding ≥400 cells per strain) were taken for each sample and processed by thresholding to generate binary images. Artifacts and cells that were clumped or ill-represented based on lighting were manually removed. The contours of the wild-type population were aligned to generate an average shape, and PCA was performed to generate a "shape model" based off principal components called "shape modes" that, together, describe at least 95% of the variation in the wild-type population. Contours of other strains were then aligned to the wild-type PCA shape model as a reference. Kolmogorov-Smirnov tests were used on each shape mode to determine whether there was a statistically significant difference in population distribution between the strains based on this wild-type shape model (53).

Phenotypic Characterization of OAP Mutants: Motility, Biofilm, Minimum Inhibitory/Bactericidal Concentrations and Cell Surface Hydrophobicity—Motility and biofilm formation assays were performed on log-phase bacterial broth cultures as described previously (19).

MIC₅₀ was determined in a 96-well plate as standing culture as described previously (84). Inocula of log-phase overnight cultures (100 μl) standardized to A₆₀₀ 0.0002 (10⁶

CFU/ml) in MH-TV and 11 μl of 10× concentrated test compound (in 2× serial dilutions) were added to each well. A₆₀₀ was measured for each well using the Varioskan Flash Multimode Plate Reader (Thermo Scientific), and MIC₅₀ was recorded as the lowest concentration of compound that reduced growth by 50% (by turbidity) relative to a positive control after 24 h.

Cell surface hydrophobicity was assessed using exponential phase bacterial broth cultures as described previously (85) with the following adjustments. Cultures were harvested at 8 000 × *g* for 10 min and washed three times with PBS. Cells were resuspended to an A₆₀₀ ~0.5 in PBS, and the absorbance was recorded. Hexadecane was added to the standardized cultures in a ratio of 1:4 hexadecane/culture by volume, vortexed for 5 min, and incubated at 38 °C for 30 min. The aqueous layer was isolated, aerated by bubbling N₂ gas through the aqueous layer for 30 s, and left open to the air for 10 min to ensure removal of all traces of hexadecane, and the A₆₀₀ was measured. Cell surface hydrophobicity was expressed as follows, where A_{600i} and A_{600f} refer to the optical densities before and after extraction, respectively.

$$\% \text{ Hydrophobicity} = \left(\frac{A_{600i} - A_{600f}}{A_{600i}} \right) \times 100\% \quad (\text{Eq. 1})$$

Chick Colonization—Chick colonization was assessed under protocol 10462 approved by the University of Michigan Committee on Care and Use of Animals, as described previously (19, 79).

Gentamicin Protection Assay for Host-Cell Infection—Gm protection assays were performed essentially as described previously (86). INT407 human epithelial cells were seeded into 24-well tissue culture plates at ~1.25 × 10⁵ cells in minimum essential medium (MEM) supplemented with 10% (v/v) FBS and 1× penicillin/streptomycin (Gibco, Life Technologies, Inc.) 24 h prior to infection. Infections were initiated by adding log-phase bacterial cultures standardized to A₆₀₀ 0.002 in MEM (1 × 10⁷ CFU/ml) and added to INT407 cells previously washed twice with 1 ml of MEM to give a multiplicity of infection of ~80. Adherence/invasion after 3 h of infection, invasion following a 2-h Gm treatment (150 μg/ml) to kill extracellular bacteria, and intracellular survival following removal of the high Gm concentration and incubation of cells in fresh medium with 10 μg/ml Gm and 3% FBS for an additional 3 h were assessed as described (86).

Interleukin-8 Quantification—The concentration of IL-8 secreted by INT407 cells either left uninfected or infected with *C. jejuni* wild-type strain 81-176, Δ*ape1*, or Δ*ape1*^C for 24 h was assayed using the human IL-8 ELISA kit (Thermo Fisher Scientific) as described previously (18).

Author Contributions—Initial conceptualization of the project details was by E. F. and E. C. G. R. H. conducted most of the experiments in the study and prepared the manuscript with E. C. G. and E. F. D. S. conducted the *O*-acetylation assays on purified PG from OAP mutants. J. B. conducted experiments on the muropeptide profiles of the OAP mutants. M. E. T. and J. G. J. conducted the chick colonization assays with OAP mutants. Oversight of the project was provided by E. C. G., A. J. C., W. V., and V. J. D. All authors reviewed and approved the final version of the manuscript.

Acknowledgment—We thank Jenny Vermeulen for technical assistance in PG sample preparations.

References

1. Yuki, N., and Hartung, H. P. (2012) Guillain-Barre syndrome. *N. Engl. J. Med.* **366**, 2294–2304
2. Jacobs, B. C., Rothbarth, P. H., van der Meché, F. G., Herbrink, P., Schmitz, P. I., de Klerk, M. A., and van Doorn, P. A. (1998) The spectrum of antecedent infections in Guillain-Barre syndrome: a case-control study. *Neurology* **51**, 1110–1115
3. Man, S. M. (2011) The clinical importance of emerging *Campylobacter* species. *Nat. Rev. Gastroenterol. Hepatol.* **8**, 669–685
4. Silva, J., Leite, D., Fernandes, M., Mena, C., Gibbs, P. A., and Teixeira, P. (2011) *Campylobacter* spp. as a foodborne pathogen: a review. *Front. Microbiol.* **2**, 200
5. Luangtongkum, T., Jeon, B., Han, J., Plummer, P., Logue, C. M., and Zhang, Q. (2009) Antibiotic resistance in *Campylobacter*: emergence, transmission and persistence. *Future Microbiol.* **4**, 189–200
6. Dasti, J. I., Tareen, A. M., Lugert, R., Zautner, A. E., and Gross, U. (2010) *Campylobacter jejuni*: a brief overview on pathogenicity-associated factors and disease-mediating mechanisms. *Int. J. Med. Microbiol.* **300**, 205–211
7. Gundogdu, O., Bentley, S. D., Holden, M. T., Parkhill, J., Dorrell, N., and Wren, B. W. (2007) Re-annotation and re-analysis of the *Campylobacter jejuni* NCTC11168 genome sequence. *BMC Genomics* **8**, 162
8. Parkhill, J., Wren, B. W., Mungall, K., Ketley, J. M., Churcher, C., Basham, D., Chillingworth, T., Davies, R. M., Feltwell, T., Holroyd, S., Jagels, K., Karlyshev, A. V., Moule, S., Pallen, M. J., Penn, C. W., et al. (2000) The genome sequence of the food-borne pathogen *Campylobacter jejuni* reveals hypervariable sequences. *Nature* **403**, 665–668
9. Louwen, R. P., van Belkum, A., Wagenaar, J. A., Doorduyn, Y., Achterberg, R., and Endtz, H. P. (2006) Lack of association between the presence of the pVir plasmid and bloody diarrhea in *Campylobacter jejuni* enteritis. *J. Clin. Microbiol.* **44**, 1867–1868
10. Tracz, D. M., Keelan, M., Ahmed-Bentley, J., Gibreel, A., Kowalewska-Grochowska, K., and Taylor, D. E. (2005) pVir and bloody diarrhea in *Campylobacter jejuni* enteritis. *Emerg. Infect. Dis.* **11**, 838–843
11. Bacon, D. J., Alm, R. A., Burr, D. H., Hu, L., Kopecko, D. J., Ewing, C. P., Trust, T. J., and Guerry, P. (2000) Involvement of a plasmid in virulence of *Campylobacter jejuni* 81-176. *Infect. Immun.* **68**, 4384–4390
12. Gaynor, E. C., Wells, D. H., MacKichan, J. K., and Falkow, S. (2005) The *Campylobacter jejuni* stringent response controls specific stress survival and virulence-associated phenotypes. *Mol. Microbiol.* **56**, 8–27
13. Szymanski, C. M., and Gaynor, E. C. (2012) How a sugary bug gets through the day: recent developments in understanding fundamental processes impacting *Campylobacter jejuni* pathogenesis. *Gut Microbes* **3**, 135–144
14. Dworkin, J. (2010) Form equals function? Bacterial shape and its consequences for pathogenesis. *Mol. Microbiol.* **78**, 792–795
15. Frirdich, E., and Gaynor, E. C. (2013) Peptidoglycan hydrolases, bacterial shape, and pathogenesis. *Curr. Opin. Microbiol.* **16**, 767–778
16. Vollmer, W. (2008) Structural variation in the glycan strands of bacterial peptidoglycan. *FEMS Microbiol. Rev.* **32**, 287–306
17. Young, K. D. (2006) The selective value of bacterial shape. *Microbiol. Mol. Biol. Rev.* **70**, 660–703
18. Frirdich, E., Biboy, J., Adams, C., Lee, J., Ellermeier, J., Giella, L. D., Dirita, V. J., Girardin, S. E., Vollmer, W., and Gaynor, E. C. (2012) Peptidoglycan-modifying enzyme Pgp1 is required for helical cell shape and pathogenicity traits in *Campylobacter jejuni*. *PLoS Pathog.* **8**, e1002602
19. Frirdich, E., Vermeulen, J., Biboy, J., Soares, F., Taveirne, M. E., Johnson, J. G., DiRita, V. J., Girardin, S. E., Vollmer, W., and Gaynor, E. C. (2014) Peptidoglycan LD-carboxypeptidase Pgp2 influences *Campylobacter jejuni* helical cell shape and pathogenic properties and provides the substrate for the DL-carboxypeptidase Pgp1. *J. Biol. Chem.* **289**, 8007–8018
20. Boneca, I. G. (2005) The role of peptidoglycan in pathogenesis. *Curr. Opin. Microbiol.* **8**, 46–53
21. Cabanes, D., Dussurget, O., Dehoux, P., and Cossart, P. (2004) Auto, a surface associated autolysin of *Listeria monocytogenes* required for entry into eukaryotic cells and virulence. *Mol. Microbiol.* **51**, 1601–1614
22. Lenz, L. L., Mohammadi, S., Geissler, A., and Portnoy, D. A. (2003) SecA2-dependent secretion of autolytic enzymes promotes *Listeria monocytogenes* pathogenesis. *Proc. Natl. Acad. Sci. U.S.A.* **100**, 12432–12437
23. Viala, J., Chaput, C., Boneca, I. G., Cardona, A., Girardin, S. E., Moran, A. P., Athman, R., Mémet, S., Huerre, M. R., Coyle, A. J., DiStefano, P. S., Sansonetti, P. J., Labigne, A., Bertin, J., Philpott, D. J., and Ferrero, R. L. (2004) Nod1 responds to peptidoglycan delivered by the *Helicobacter pylori* cag pathogenicity island. *Nat. Immunol.* **5**, 1166–1174
24. Vollmer, W., and Tomasz, A. (2002) Peptidoglycan N-acetylglucosamine deacetylase, a putative virulence factor in *Streptococcus pneumoniae*. *Infect. Immun.* **70**, 7176–7178
25. Schoonmaker, M. K., Bishai, W. R., and Lamichhane, G. (2014) Nonclassical transpeptidases of *Mycobacterium tuberculosis* alter cell size, morphology, the cytosolic matrix, protein localization, virulence, and resistance to beta-lactams. *J. Bacteriol.* **196**, 1394–1402
26. Strating, H., Vandenende, C., and Clarke, A. J. (2012) Changes in peptidoglycan structure and metabolism during differentiation of *Proteus mirabilis* into swarmer cells. *Can. J. Microbiol.* **58**, 1183–1194
27. Sycuro, L. K., Pincus, Z., Gutierrez, K. D., Biboy, J., Stern, C. A., Vollmer, W., and Salama, N. R. (2010) Peptidoglycan crosslinking relaxation promotes *Helicobacter pylori*'s helical shape and stomach colonization. *Cell* **141**, 822–833
28. Sycuro, L. K., Wyckoff, T. J., Biboy, J., Born, P., Pincus, Z., Vollmer, W., and Salama, N. R. (2012) Multiple peptidoglycan modification networks modulate *Helicobacter pylori*'s cell shape, motility, and colonization potential. *PLoS Pathog.* **8**, e1002603
29. Moynihan, P. J., and Clarke, A. J. (2013) Assay for peptidoglycan O-acetyltransferase: a potential new antibacterial target. *Anal. Biochem.* **439**, 73–79
30. Moynihan, P. J., and Clarke, A. J. (2014) Substrate specificity and kinetic characterization of peptidoglycan O-acetyltransferase B from *Neisseria gonorrhoeae*. *J. Biol. Chem.* **289**, 16748–16760
31. Pfeffer, J. M., and Clarke, A. J. (2012) Identification of the first known inhibitors of O-acetylpeptidoglycan esterase: a potential new antibacterial target. *Chembiochem* **13**, 722–731
32. Pfeffer, J. M., Weadge, J. T., and Clarke, A. J. (2013) Mechanism of action of *Neisseria gonorrhoeae* O-acetylpeptidoglycan esterase, an SGNH serine esterase. *J. Biol. Chem.* **288**, 2605–2613
33. Veyrier, F. J., Williams, A. H., Mesnage, S., Schmitt, C., Taha, M. K., and Boneca, I. G. (2013) De-O-acetylation of peptidoglycan regulates glycan chain extension and affects *in vivo* survival of *Neisseria meningitidis*. *Mol. Microbiol.* **87**, 1100–1112
34. Rosenthal, R. S., Blundell, J. K., and Perkins, H. R. (1982) Strain-related differences in lysozyme sensitivity and extent of O-acetylation of gonococcal peptidoglycan. *Infect. Immun.* **37**, 826–829
35. Bera, A., Biswas, R., Herbert, S., and Götz, F. (2006) The presence of peptidoglycan O-acetyltransferase in various staphylococcal species correlates with lysozyme resistance and pathogenicity. *Infect. Immun.* **74**, 4598–4604
36. Moynihan, P. J., Sychantha, D., and Clarke, A. J. (2014) Chemical biology of peptidoglycan acetylation and deacetylation. *Bioorg. Chem.* **54**, 44–50
37. Wang, G., Lo, L. F., Forsberg, L. S., and Maier, R. J. (2012) *Helicobacter pylori* peptidoglycan modifications confer lysozyme resistance and contribute to survival in the host. *mBio* **3**, e00409–00412
38. Ellison, R. T., 3rd, and Giehl, T. J. (1991) Killing of Gram-negative bacteria by lactoferrin and lysozyme. *J. Clin. Invest.* **88**, 1080–1091
39. Ellison, R. T., 3rd, Giehl, T. J., and LaForce, F. M. (1988) Damage of the outer membrane of enteric Gram-negative bacteria by lactoferrin and transferrin. *Infect. Immun.* **56**, 2774–2781
40. Fleming, T. J., Wallsmith, D. E., and Rosenthal, R. S. (1986) Arthropathic properties of gonococcal peptidoglycan fragments: implications for the pathogenesis of disseminated gonococcal disease. *Infect. Immun.* **52**, 600–608

41. Moynihan, P. J., and Clarke, A. J. (2011) O-Acetylated peptidoglycan: controlling the activity of bacterial autolysins and lytic enzymes of innate immune systems. *Int. J. Biochem. Cell Biol.* **43**, 1655–1659
42. Weadge, J. T., Pfeffer, J. M., and Clarke, A. J. (2005) Identification of a new family of enzymes with potential O-acetylpeptidoglycan esterase activity in both Gram-positive and Gram-negative bacteria. *BMC Microbiol.* **5**, 49
43. Weadge, J. T., and Clarke, A. J. (2006) Identification and characterization of O-acetylpeptidoglycan esterase: a novel enzyme discovered in *Neisseria gonorrhoeae*. *Biochemistry* **45**, 839–851
44. Dillard, J. P., and Hackett, K. T. (2005) Mutations affecting peptidoglycan acetylation in *Neisseria gonorrhoeae* and *Neisseria meningitidis*. *Infect. Immun.* **73**, 5697–5705
45. Weadge, J. T., and Clarke, A. J. (2007) *Neisseria gonorrhoeae* O-acetylpeptidoglycan esterase, a serine esterase with a Ser-His-Asp catalytic triad. *Biochemistry* **46**, 4932–4941
46. Williams, A. H., Veyrier, F. J., Bonis, M., Michaud, Y., Raynal, B., Taha, M. K., White, S. W., Haouz, A., and Boneca, I. G. (2014) Visualization of a substrate-induced productive conformation of the catalytic triad of the *Neisseria meningitidis* peptidoglycan O-acetyltransferase reveals mechanistic conservation in SGNH esterase family members. *Acta Crystallogr. D Biol. Crystallogr.* **70**, 2631–2639
47. Ménard, R., Sansonetti, P. J., and Parsot, C. (1993) Nonpolar mutagenesis of the *ipa* genes defines IpaB, IpaC, and IpaD as effectors of *Shigella flexneri* entry into epithelial cells. *J. Bacteriol.* **175**, 5899–5906
48. Karlyshev, A. V., and Wren, B. W. (2005) Development and application of an Insertional system for gene delivery and expression in *Campylobacter jejuni*. *Appl. Environ. Microbiol.* **71**, 4004–4013
49. Clarke, A. J. (1993) Compositional analysis of peptidoglycan by high-performance anion-exchange chromatography. *Anal. Biochem.* **212**, 344–350
50. Clarke, A. J. (1993) Extent of peptidoglycan O-acetylation in the tribe proteaeae. *J. Bacteriol.* **175**, 4550–4553
51. Dupont, C., and Clarke, A. J. (1991) Dependence of lysozyme-catalysed solubilization of *Proteus mirabilis* peptidoglycan on the extent of O-acetylation. *Eur. J. Biochem.* **195**, 763–769
52. Scheurwater, E., Reid, C. W., and Clarke, A. J. (2008) Lytic transglycosylases: bacterial space-making autolysins. *Int. J. Biochem. Cell Biol.* **40**, 586–591
53. Pincus, Z., and Theriot, J. A. (2007) Comparison of quantitative methods for cell-shape analysis. *J. Microsc.* **227**, 140–156
54. Lin, M. F., Lucas, H. C., and Shmueli, G. (2013) Too big to fail: large samples and the *p*-value problem. *Inform. Syst. Res.* **24**, 906–917
55. Lertsethtakarn, P., Ottemann, K. M., and Hendrixson, D. R. (2011) Motility and chemotaxis in *Campylobacter* and *Helicobacter*. *Annu. Rev. Microbiol.* **65**, 389–410
56. Buswell, C. M., Herlihy, Y. M., Lawrence, L. M., McGuiggan, J. T., Marsh, P. D., Keevil, C. W., and Leach, S. A. (1998) Extended survival and persistence of *Campylobacter* spp. in water and aquatic biofilms and their detection by immunofluorescent-antibody and -rRNA staining. *Appl. Environ. Microbiol.* **64**, 733–741
57. McLennan, M. K., Ringoir, D. D., Fridrich, E., Svensson, S. L., Wells, D. H., Jarrell, H., Szymanski, C. M., and Gaynor, E. C. (2008) *Campylobacter jejuni* biofilms up-regulated in the absence of the stringent response utilize a calcofluor white-reactive polysaccharide. *J. Bacteriol.* **190**, 1097–1107
58. Joshua, G. W., Guthrie-Irons, C., Karlyshev, A. V., and Wren, B. W. (2006) Biofilm formation in *Campylobacter jejuni*. *Microbiology* **152**, 387–396
59. Rosenberg, M., Gutnick, D., and Rosenberg, E. (1980) Adherence of bacteria to hydrocarbons—a simple method for measuring cell-surface hydrophobicity. *FEMS Microbiol. Lett.* **9**, 29–33
60. Everest, P. H., Goossens, H., Butzler, J. P., Lloyd, D., Knutton, S., Ketley, J. M., and Williams, P. H. (1992) Differentiated Caco-2 cells as a model for enteric invasion by *Campylobacter jejuni* and *C. coli*. *J. Med. Microbiol.* **37**, 319–325
61. Bacon, D. J., Szymanski, C. M., Burr, D. H., Silver, R. P., Alm, R. A., and Guerry, P. (2001) A phase-variable capsule is involved in virulence of *Campylobacter jejuni* 81-176. *Mol. Microbiol.* **40**, 769–777
62. Moynihan, P. J., and Clarke, A. J. (2010) O-Acetylation of peptidoglycan in Gram-negative bacteria: identification and characterization of peptidoglycan O-acetyltransferase in *Neisseria gonorrhoeae*. *J. Biol. Chem.* **285**, 13264–13273
63. Romeis, T., and Höltje, J. V. (1994) Specific interaction of penicillin-binding proteins 3 and 7/8 with soluble lytic transglycosylase in *Escherichia coli*. *J. Biol. Chem.* **269**, 21603–21607
64. Vollmer, W., von Rechenberg, M., and Höltje, J. V. (1999) Demonstration of molecular interactions between the murein polymerase PBP1B, the lytic transglycosylase MltA, and the scaffolding protein MipA of *Escherichia coli*. *J. Biol. Chem.* **274**, 6726–6734
65. Clarke, A. J., and Dupont, C. (1992) O-Acetylated peptidoglycan: its occurrence, pathobiological significance, and biosynthesis. *Can. J. Microbiol.* **38**, 85–91
66. Mattei, P. J., Neves, D., and Dessen, A. (2010) Bridging cell wall biosynthesis and bacterial morphogenesis. *Curr. Opin. Struct. Biol.* **20**, 749–755
67. Scyuro, L. K., Rule, C. S., Petersen, T. W., Wyckoff, T. J., Sessler, T., Nagarkar, D. B., Khalid, F., Pincus, Z., Biboy, J., Vollmer, W., and Salama, N. R. (2013) Flow cytometry-based enrichment for cell shape mutants identifies multiple genes that influence *Helicobacter pylori* morphology. *Mol. Microbiol.* **90**, 869–883
68. Hizukuri, Y., Kojima, S., Yakushi, T., Kawagishi, I., and Homma, M. (2008) Systematic Cys mutagenesis of FlgI, the flagellar P-ring component of *Escherichia coli*. *Microbiology* **154**, 810–817
69. Jones, C. J., Homma, M., and Macnab, R. M. (1989) L-, P-, and M-ring proteins of the flagellar basal body of *Salmonella typhimurium*: gene sequences and deduced protein sequences. *J. Bacteriol.* **171**, 3890–3900
70. Roujeinikova, A. (2008) Crystal structure of the cell wall anchor domain of MotB, a stator component of the bacterial flagellar motor: implications for peptidoglycan recognition. *Proc. Natl. Acad. Sci. U.S.A.* **105**, 10348–10353
71. Morimoto, Y. V., Nakamura, S., Hiraoka, K. D., Namba, K., and Minamino, T. (2013) Distinct roles of highly conserved charged residues at the MotA-FlgI interface in bacterial flagellar motor rotation. *J. Bacteriol.* **195**, 474–481
72. Roman, S. J., Meyers, M., Volz, K., and Matsumura, P. (1992) A chemotactic signaling surface on CheY defined by suppressors of flagellar switch mutations. *J. Bacteriol.* **174**, 6247–6255
73. Kanungpean, D., Kakuda, T., and Takai, S. (2011) False-positive responses of *Campylobacter jejuni* when using the chemical-in-plug chemotaxis assay. *J. Vet. Med. Sci.* **73**, 389–391
74. McGee, D. J., Langford, M. L., Watson, E. L., Carter, J. E., Chen, Y. T., and Ottemann, K. M. (2005) Colonization and inflammation deficiencies in Mongolian gerbils infected by *Helicobacter pylori* chemotaxis mutants. *Infect. Immun.* **73**, 1820–1827
75. Roue, S., Bonis, M., Chaput, C., Ecobichon, C., Mattox, A., Barrière, C., Geldmacher, N., Guadagnini, S., Schmitt, C., Prévost, M. C., Labigne, A., Backert, S., Ferrero, R. L., and Boneca, I. G. (2012) Peptidoglycan maturation enzymes affect flagellar functionality in bacteria. *Mol. Microbiol.* **86**, 845–856
76. Svensson, S. L., Pryjma, M., and Gaynor, E. C. (2014) Flagella-mediated adhesion and extracellular DNA release contribute to biofilm formation and stress tolerance of *Campylobacter jejuni*. *PLoS ONE* **9**:e106063
77. Godlewska, R., Wiśniewska, K., Pietras, Z., and Jagusztyn-Krynicka, E. K. (2009) Peptidoglycan-associated lipoprotein (Pal) of Gram-negative bacteria: function, structure, role in pathogenesis and potential application in immunoprophylaxis. *FEMS Microbiol. Lett.* **298**, 1–11
78. Hizukuri, Y., Morton, J. F., Yakushi, T., Kojima, S., and Homma, M. (2009) The peptidoglycan-binding (PGB) domain of the *Escherichia coli* pal protein can also function as the PGB domain in *E. coli* flagellar motor protein MotB. *J. Biochem.* **146**, 219–229
79. Hendrixson, D. R., and DiRita, V. J. (2004) Identification of *Campylobacter jejuni* genes involved in commensal colonization of the chick gastrointestinal tract. *Mol. Microbiol.* **52**, 471–484
80. Hayashi, K. (1975) A rapid determination of sodium dodecyl sulfate with methylene blue. *Anal. Biochem.* **67**, 503–506
81. Glauner, B. (1988) Separation and quantification of mucopeptides with high-performance liquid-chromatography. *Anal. Biochem.* **172**, 451–464

Role of *C. jejuni* Peptidoglycan O-Acetylation

82. Bui, N. K., Gray, J., Schwarz, H., Schumann, P., Blanot, D., and Vollmer, W. (2009) The peptidoglycan sacculus of *Myxococcus xanthus* has unusual structural features and is degraded during glycerol-induced myxospore development. *J. Bacteriol.* **191**, 494–505
83. Petersen, T. N., Brunak, S., von Heijne, G., and Nielsen, H. (2011) SignalP 4.0: discriminating signal peptides from transmembrane regions. *Nat. Methods* **8**, 785–786
84. Hancock, R. E. (1999) *Hancock Laboratory Methods*, Department of Microbiology and Immunology, University of British Columbia, British Columbia, Canada
85. Ben Abdallah, F., Lagha, R., Said, K., Kallel, H., and Gharbi, J. (2014) Detection of cell surface hydrophobicity, biofilm and fimbriae genes in *Salmonella* isolated from tunisian clinical and poultry meat. *Iran J. Public Health* **43**, 423–431
86. Pryjma, M., Apel, D., Huynh, S., Parker, C. T., and Gaynor, E. C. (2012) FdhTU-modulated formate dehydrogenase expression and electron donor availability enhance recovery of *Campylobacter jejuni* following host cell infection. *J. Bacteriol.* **194**, 3803–3813
87. Korlath, J. A., Osterholm, M. T., Judy, L. A., Forfang, J. C., and Robinson, R. A. (1985) A point-source outbreak of campylobacteriosis associated with consumption of raw milk. *J. Infect. Dis.* **152**, 592–596
88. Glauner, B., Hölzle, J. V., and Schwarz, U. (1988) The composition of the murein of *Escherichia coli*. *J. Biol. Chem.* **263**, 10088–10095